SANDIA REPORT
SAND2014-20095
Unlimited Release
Printed November 2014

A Parametric Study of Rate of Advance and Area Coverage Rate Performance of Synthetic Aperture Radar

Ann Marie Raynal, Bryan L. Burns, Armin W. Doerry, and William H. Hensley, Jr.

Prepared by
Sandia National Laboratories
Albuquerque, New Mexico 87185 and Livermore, California 94550

Sandia National Laboratories is a multi-program laboratory managed and operated by Sandia Corporation, a wholly owned subsidiary of Lockheed Martin Corporation, for the U.S. Department of Energy's National Nuclear Security Administration under contract DE-AC04-94AL85000.

Sandia National Laboratories

Issued by Sandia National Laboratories, operated for the United States Department of Energy by Sandia Corporation.

Printed in the United States of America. This report has been reproduced directly from the best available copy.

Available to DOE and DOE contractors from
U.S. Department of Energy
Office of Scientific and Technical Information
P.O. Box 62
Oak Ridge, TN 37831

Telephone: (865) 576-8401
Facsimile: (865) 576-5728
E-Mail: reports@adonis.osti.gov
Online ordering: http://www.osti.gov/bridge

Available to the public from
U.S. Department of Commerce
National Technical Information Service
5285 Port Royal Rd.
Springfield, VA 22161

Telephone: (800) 553-6847
Facsimile: (703) 605-6900
E-Mail: orders@ntis.fedworld.gov
Online order: http://www.ntis.gov/help/ordermethods.asp?loc=7-4-0#online

SAND2014-20095
Unlimited Release
Printed November 2014

A Parametric Study of Rate of Advance and Area Coverage Rate Performance of Synthetic Aperture Radar

Ann Marie Raynal, MS0519
William H. Hensley, Jr., MS0532
ISR Analysis & Applications Department

Bryan L. Burns
RF & Electronic Systems Center, MS0532

Armin W. Doerry
ISR Mission Engineering Department, MS0519

Sandia National Laboratories
P.O. Box 5800
Albuquerque, New Mexico 87185-MSXXXX

Abstract

The linear ground distance per unit time and ground area covered per unit time of producing synthetic aperture radar (SAR) imagery, termed rate of advance (ROA) and area coverage rate (ACR), are important metrics for platform and radar performance in surveillance applications. These metrics depend on many parameters of a SAR system such as wavelength, aircraft velocity, resolution, antenna beamwidth, imaging mode, and geometry. Often the effects of these parameters on rate of advance and area coverage rate are non-linear. This report addresses the impact of different parameter spaces as they relate to rate of advance and area coverage rate performance.

ACKNOWLEDGMENTS

The authors are greatly indebted to Jeffrey D. Bradley for his detailed advice on how best to data-mine radar sensor segment length information. We would also like to thank Douglas G. Thompson, for providing guidance regarding existing work related to area coverage rate within Sandia National Laboratories, and Douglas L. Bickel, for insightful conversations on system engineering choices regarding pixel- and beam-limited range swath, among other topics.

CONTENTS

FIGURES

TABLES

NOMENCLATURE

ACR	Area Coverage Rate
ADC	Analog-to-Digital Converter
DOE	Department of Energy
FFT	Fast Fourier Transform
GMT	Greenwich Mean Time
GPS	Global Positioning System
IF	Intermediate Frequency
IMU	Inertial Measurement Unit
IPR	Impulse Response
ISR	Intelligence, Surveillance, and Reconnaissance
LFM	Linear frequency-modulated
MCP	Motion Compensation Point
NCDC	National Climatic Data Center
NOAA	National Oceanographic and Atmospheric Administration
RF	Radio-frequency
ROA	Rate of Advance
SAR	Synthetic Aperture Radar
SNL	Sandia National Laboratories

“Prejudice squints when it looks, and lies when it talks.”

- *Duchess de Abrantes*

1. INTRODUCTION

As airborne intelligence, surveillance, and reconnaissance (ISR) systems tasked to serve the needs of the warfighter increase over an area, so does the need for effective and efficient management of finite operational resources. These resources can be the aircraft, fuel, sensors, runways and airspace, supporting analysis and exploitation framework, the frequency spectrum or the like. Some constraints are physical or based on available materiel and personnel, but others are based on sensor capability and engineering design choices.

Aircraft operational costs, particularly platform advance rates, relative to successful mission executions are a significant financial consideration when comparing airborne sensor assets that meet specific warfighter needs. A sensor that can provide greater mission (or multi-mission) performance per unit area per unit time (or ultimately operational dollar) is more cost-effective and thus more valuable as an ISR asset. Thus sensors with greater imaging area coverage or platform advance per unit time reduce the flight operational cost per square kilometer of a mission considerably, if all else is equal.

The linear ground distance per unit time and ground area covered per unit time of producing synthetic aperture radar (SAR) imagery, termed rate of advance (ROA) and area coverage rate (ACR), are important metrics for platform and radar performance in ISR applications for the aforementioned operational cost and limited resource reasons. These metrics depend on many parameters of a SAR system such as wavelength, aircraft velocity, resolution, antenna beamwidth, imaging mode, and geometry. Often the effects of these parameters on rate of advance and area coverage rate are non-linear. This report addresses the impact of different parameter spaces as they relate to rate of advance and area coverage rate performance.

This report is organized as follows. Chapter 2 details the mathematical theory behind area coverage rate and rate of advance for the general case of squinted geometries for the imaging of a single patch and describes single patch performance. Chapter 3 discusses multi-patch trajectory and mission performance for squinted and broadside geometries with varying antenna size, resolution, and grazing angle requirements. Conclusions are provided in Chapter 4.

"To raise new questions, new possibilities, to regard old problems from a new angle, requires creative imagination and marks real advance in science."

- Albert Einstein

2. SINGLE IMAGE RATE OF ADVANCE AND AREA COVERAGE RATE THEORY

The linear rate of advance and area coverage rate for imaging a single patch will be dependent on the image dimensions, as well as the time taken to form the image. In other words, the image ground range and cross-range swath, as well as the synthetic aperture time, need to be determined to understand the performance metrics of linear rate of advance and area coverage rate, i.e.,

$$\dot{L} = \frac{XR_{swath}}{T_a}, \text{ and} \tag{1}$$

$$\dot{A} = \frac{R_{swath} XR_{swath}}{T_a}. \tag{2}$$

The high-level geometry and parameter relationships for ROA and ACR are shown in Figure 1. The synthetic aperture time will depend on the synthetic aperture length and platform ground speed. Finding the ground range and cross-range swath, synthetic aperture length, and platform ground speed are non-trivial. This chapter develops the mathematical considerations for these parameters to understand the factors that will impact radar system performance in rate of advance and area coverage rate.

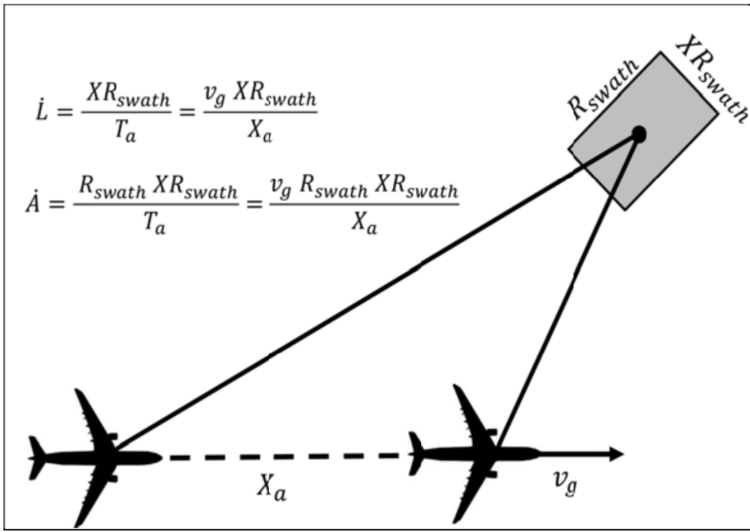

Symbol	Units	Description
$\dot{L}$	m/s	Rate of advance
$\dot{A}$	m^2/s	Area coverage rate
X_a	m	Synthetic aperture length
T_a	s	Synthetic aperture time
v_g	m/s	Platform ground speed
R_{swath}	m	Range swath
XR_{swath}	m	Cross-range swath

Figure 1. Single Image Linear Rate of Advance and Area Coverage Rate

Many approaches exist to determine rate of advance and area coverage rate. The method outlined herein is by no means the only or most rigorous approach, as the developments assume a flat earth and antenna 3-dB beamwidths for the ground swath footprint size.

2.1. Squint Mode Platform Geometry and Parameter Relationships

Figure 2 shows the general squint mode platform geometry we are interested in understanding, with corresponding parameter definitions. We assume that the platform height above ground level, nominal grazing angle for broadside geometry, and nominal ground squint angle at aperture center are provided.

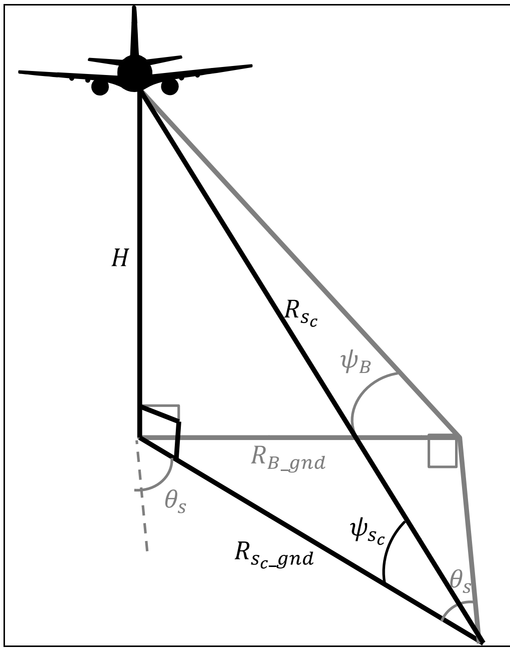

Symbol	***Units***	***Description***
H	m	Platform height above ground level (AGL)
ψ_B	radians	Nominal grazing angle at broadside
ψ_{s_c}	radians	Nominal grazing angle at squinted aperture center
θ_s	radians	Nominal ground squint angle at aperture center
R_{B_gnd}	m	Ground range at broadside
R_{s_c}	m	Slant range at squinted aperture center
$R_{s_c\_gnd}$	m	Ground range at squinted aperture center

Figure 2. Squint Mode Platform Geometry

With some foresight, we are interested in finding the ground and slant range at the squinted aperture center, as well as the nominal grazing angle at the squinted aperture center. These parameters will be necessary for determining the range and cross-range swath sizes, and the synthetic aperture length.

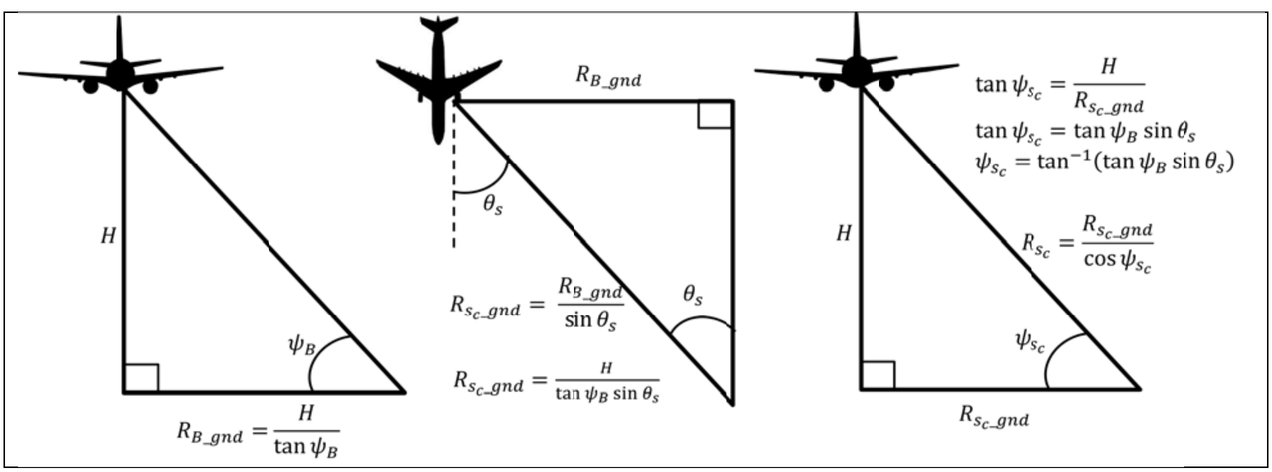

Figure 3. Squint Mode Platform Geometry Parameter Relationships

Figure 3 shows right triangle relationships that may be utilized to find these parameter relationships. We first find the broadside ground range from the platform height and nominal broadside grazing angle. This relationship is leveraged to find the ground range at the squinted aperture center from the ground squint angle at aperture center. Once this parameter is known, the nominal grazing angle at the squinted aperture center can be found, which then yields the slant range at the squinted aperture center. To summarize, the nominal grazing angle and ground and slant range at the squinted aperture center are:

$$\psi_{s_c} = \tan^{-1}(\tan\psi_B \sin\theta_s), \tag{3}$$

$$R_{s_c\_gnd} = \frac{H}{\tan\psi_B \sin\theta_s}, \text{ and} \tag{4}$$

$$R_{s_c} = \frac{R_{s_c\_gnd}}{\cos\psi_{s_c}}. \tag{5}$$

2.2. Squint Mode Ground Range Swath

The ground range swath of a radar system may be range pixel- or beam-limited. This subsection details the two types of limitations. The 3-dB beamwidth of the antenna is assumed for the calculations of range beam swath. Ultimately the smallest or minimum swath coverage of the two limitations is assumed, that is:

$$R_{swath_{lim}} = \min\left\{R_{swath_{\theta EL3dBlim}}, R_{swath_{pixlim}}\right\}, \tag{6}$$

where $R_{swath_{lim}}$, $R_{swath_{\theta EL3dBlim}}$, and $R_{swath_{pixlim}}$ are the final-, beam-, and pixel-limited ground range swaths in meters.

2.2.1. Ground Range Beam-Limited Swath

The range beam-limited swath of a radar system is dependent on the elevation beamwidth of the antenna and the slant range and nominal grazing angle at the squinted aperture center. The 3-dB elevation beamwidth of the antenna is given by the wavelength at the center frequency in meters, λ_c, the physical width of the antenna in meters, W_a, and any windowing that may be applied to the illumination pattern:

$$\theta_{EL_{3dB}} = \frac{\lambda_c k_0}{W_a}. \tag{7}$$

Figure 4 shows the platform geometry for determining the beam-limited ground range swath which entails the physical length covered by the antenna beamwidth footprint on the ground at the squinted aperture center. Due to the squinted nature of the geometry, asymmetric near and far range swath segments will compose the total swath,

$$R_{swath_{\theta EL3dBlim}} = R_{swath\_near_{3dB}} + R_{swath\_far_{3dB}}. \tag{8}$$

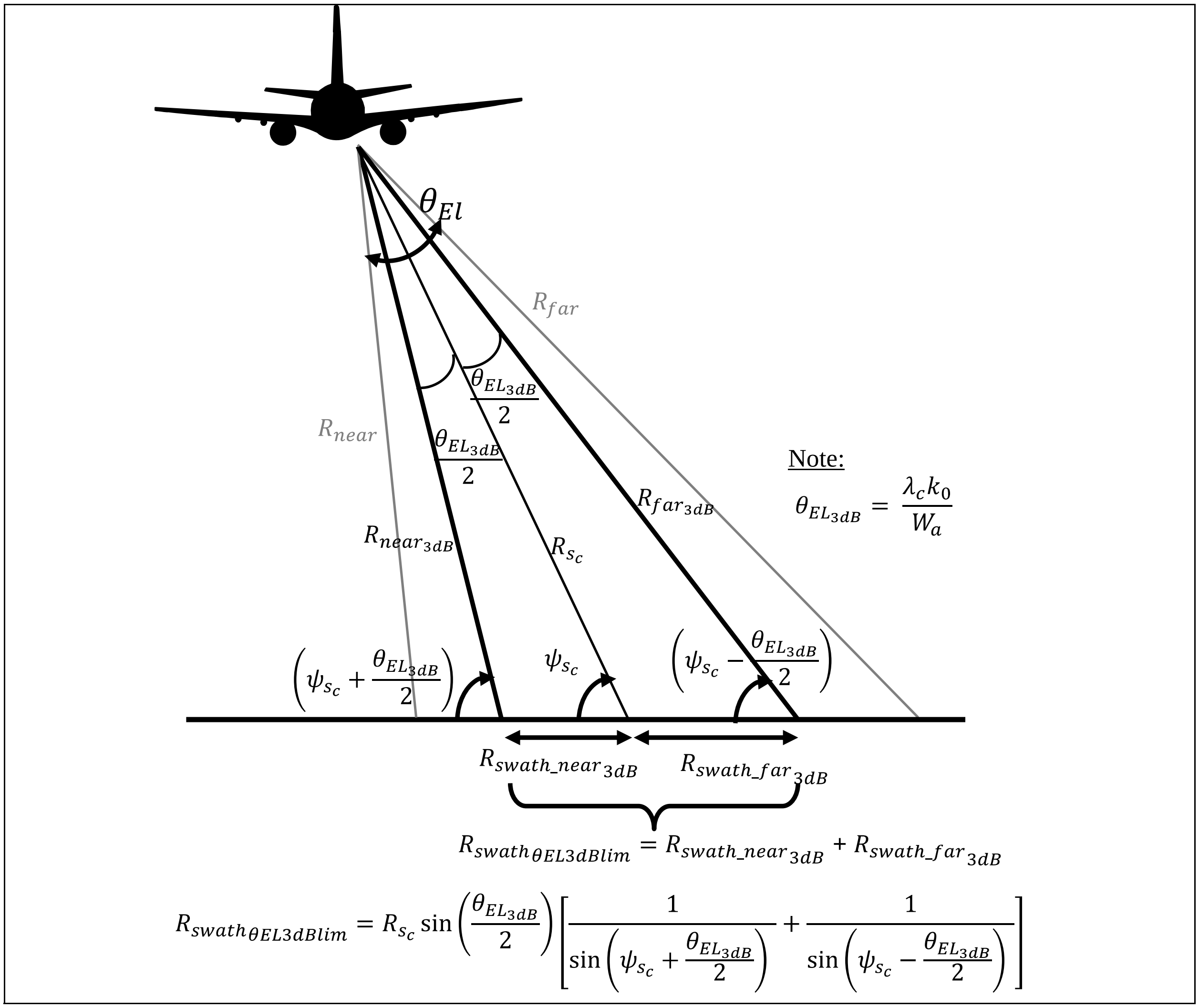

Figure 4. Beam-limited Range Swath

These segments can be found using the law of sines and the trigonometric identity for the sine of the difference of two angles, i.e.,

$$\frac{\sin a}{A} = \frac{\sin b}{B}, \text{ and} \tag{9}$$

$$\sin(a - b) = \sin a \cos b - \cos a \sin b, \tag{10}$$

where a and b are angles and A and B are the opposite sides of the triangle from these angles, respectively. We note, for example, that the $\sin(\pi - b) = \sin \pi \cos b - \cos \pi \sin b = \sin b$.

Thus, the far range swath segment is given by the law of sines as:

$$\frac{\sin\left(\psi_{s_c} - \frac{\theta_{EL_{3dB}}}{2}\right)}{R_{s_c}} = \frac{\sin\left(\frac{\theta_{EL_{3dB}}}{2}\right)}{R_{swath\_far_{3dB}}},$$

which yields $$R_{swath\_far_{3dB}} = \frac{R_{s_c} \sin\left(\frac{\theta_{EL_{3dB}}}{2}\right)}{\sin\left(\psi_{s_c} - \frac{\theta_{EL_{3dB}}}{2}\right)}. \quad (11)$$

The near range swath segment is given by the law of sines as:

$$\frac{\sin\left(\pi - \left(\psi_{s_c} + \frac{\theta_{EL_{3dB}}}{2}\right)\right)}{R_{s_c}} = \frac{\sin\left(\frac{\theta_{EL_{3dB}}}{2}\right)}{R_{swath\_near_{3dB}}},$$

which yields $$R_{swath\_near_{3dB}} = \frac{R_{s_c} \sin\left(\frac{\theta_{EL_{3dB}}}{2}\right)}{\sin\left(\pi - \left(\psi_{s_c} + \frac{\theta_{EL_{3dB}}}{2}\right)\right)}.$$

The near range swath then simplifies using the aforementioned trigonometric identity to:

$$R_{swath\_near_{3dB}} = \frac{R_{s_c} \sin\left(\frac{\theta_{EL_{3dB}}}{2}\right)}{\sin\left(\psi_{s_c} + \frac{\theta_{EL_{3dB}}}{2}\right)}. \quad (12)$$

In short, the total 3-dB beam-limited ground range swath by substitution of Equation 11 and Equation 12 into Equation 8 and simplification is:

$$R_{swath_{\theta EL3dBlim}} = R_{s_c} \sin\left(\frac{\theta_{EL_{3dB}}}{2}\right)\left[\frac{1}{\sin\left(\psi_{s_c} + \frac{\theta_{EL_{3dB}}}{2}\right)} + \frac{1}{\sin\left(\psi_{s_c} - \frac{\theta_{EL_{3dB}}}{2}\right)}\right], \quad (13)$$

where $R_{swath_{\theta EL3dBlim}} \rightarrow \infty$ if $\psi_{s_c} \leq \frac{\theta_{EL_{3dB}}}{2}$.

Note: The range swath may be extended in some modes by employing regions of the antenna beam outside of the 3-dB beamwidth. This is a design choice and the reader is referred to the literature for additional information [6].

2.2.2. Stretch Processing Ground Range Pixel-Limited Swath

The pixel-limited range swath of a radar system that employs stretch processing is dependent on the number of Fast Fourier Transform (FFT) samples utilized for processing, range pixel spacing, and characteristics of the intermediate frequency (IF) band-limiting filter. Figure 5 shows the pertinent timing information for computing the pixel-limited ground range swath. A linear frequency-modulated (LFM) chirp is transmitted by the radar, which backscatters from the scene content at the near- through far-range of the antenna beam footprint. The chirp returns are mixed and down-converted with a LFM local oscillator signal at the receiver, which “deramps” the chirp to an intermediate frequency. At the IF, the echo returns are band-pass filtered by an analog filter. Finally, an analog-to-digital converter (ADC) digitizes the band-limited echoes which are then converted to baseband where a fast Fourier transform (FFT) is applied to convert the data from frequency into range.

The roundtrip time delay in seconds for a transmitted pulse to cover the slant range swath or scene extent is given by:

$$T_{swath} = \frac{2(R_{far} - R_{near})}{c} = \frac{2R'_{swath\theta EL}}{c}, \tag{14}$$

where c is the speed of light in m/s.

The radio-frequency (RF) bandwidth of the transmitted LFM chirp is the product of the chirp rate and the pulse duration:

$$\beta_{pulse} = \gamma_{chirp} T_{pulse}. \tag{15}$$

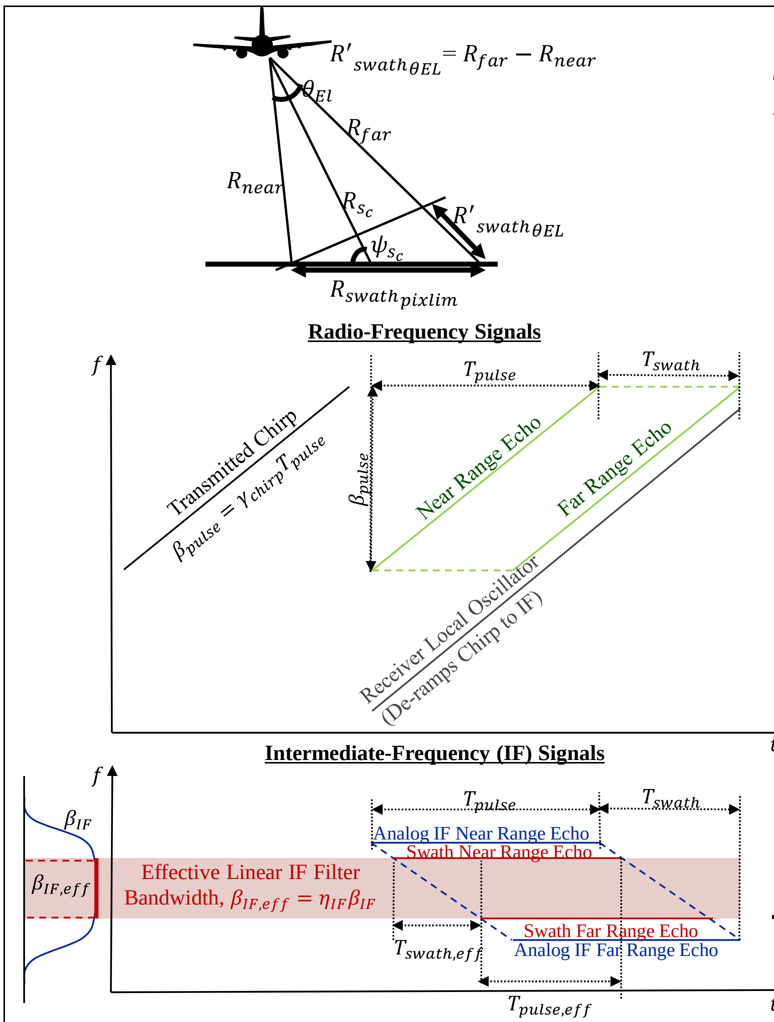

Symbol	Units	Description
T_{pulse}	s	Pulse duration
T_{swath}	s	Duration of pulse echo returns within the antenna beam
β_{pulse}	Hz	Pulse RF bandwidth
γ_{chirp}	Hz/s	Chirp rate
$T_{pulse,eff}$	s	Pulse duration kept at the IF
$T_{swath,eff}$	s	Duration of pulse echo returns kept at the IF
β_{IF}	Hz	IF filter bandwidth
$\beta_{IF,eff}$	Hz	Flat response of IF filter bandwidth
η_{IF}	-	IF filter bandwidth efficiency
$R'_{swath\theta EL}$	m	Ideal slant range swath
$R_{swath_{pixlim}}$	m	Ground range pixel-limited swath

Figure 5. Pixel-limited Range Swath

Unfortunately, radar system limitations and processing practices affect the ideal slant range swath and pulse duration at the IF. Roll-off characteristics at the edges of the non-ideal analog band-pass IF filter upon reception of the radar signal can degrade image quality by introducing ambiguities. To avoid this, the IF bandwidth post-filter is truncated to an effective width that keeps within the flat region of the filter frequency response by some factor, η_{IF}. This truncation in turn shortens the effective range swath per the figure as:

$$\beta_{IF,eff} = \eta_{IF}\beta_{IF} = \gamma_{chirp}T_{swath,eff}. \tag{16}$$

Furthermore, the time interval over which the ADC acquires samples is constrained to the region where the near and far range echoes have data in common in order to avoid increased sidelobes from asymmetric nulls (or effectively unanticipated zero-padding of the FFT) over the effective IF bandwidth. This truncation in turn shortens the effective pulse duration, thus impacting range resolution.

That is, the slant range resolution of the radar system is based on the effective RF bandwidth of the chirp and any windowing during processing to achieve lower side-lobe level characteristics of the impulse response (IPR) at the expense of a wider mainlobe (i.e. coarser resolution). Hence slant range resolution is given by:

$$\rho_r = \frac{ck_0}{2\beta_{pulse,eff}} = \frac{ck_0}{2\gamma_{chirp}T_{pulse,eff}}, \tag{17}$$

where k_0 is the window mainlobe broadening factor of the IPR, and $\beta_{pulse,eff}$ is the effective radar RF bandwidth, which can be related by the chirp rate to the effective pulse duration, $T_{pulse,eff}$, per the figure.

Note: Other radar receiver considerations outside the scope of this work may further decrease the effective pulse duration.

The slant range pixel spacing in an image is often the result of oversampling the resolution to provide finer interpolation of the IPR during processing. The slant range pixel spacing is related to the slant range resolution by:

$$\Delta r = \frac{\rho_r}{K_a}, \tag{18}$$

where K_a is the IPR oversample factor and $k_0 \leq K_a \geq 1$. Note that any window function with meaningful sidelobe reduction characteristics will have k_0 and K_a values that approach 1.

Considering single-side-band signals, the number of ADC samples required to obey Nyquist sampling of the IF echoes over the effective pulse duration is related to the ADC sampling rate, Δf_{ADC}, by:

$$N_{fast} = T_{pulse,eff}\Delta f_{\mathrm{ADC}}. \tag{19}$$

Additionally, the number of FFT samples is often fixed due to processor memory or speed limitations to some length, N_{FFT}. This value is related to the ADC fast time samples for convenience and with some foresight by:

$$N_{fast} = \frac{k_0}{K_a} N_{FFT}. \quad (20)$$

For the purposes of this study, we keep to ground plane processing. Any ground range parameter is assumed as the projection of the slant range value at the nominal grazing angle at the squinted aperture center. The effective ground range swath by Equation 15 should thus be:

$$R_{swath_{pixlim}} = \frac{c}{2\cos\psi_{s_c}} T_{swath,eff}, \quad (21)$$

By sequential substitution of Equations 16-20 into Equation 21, we observe that:

$$R_{swath_{pixlim}} = \frac{c}{2\cos\psi_{s_c}} T_{swath,eff} = \frac{c\beta_{swath,eff}}{2\gamma_{chirp}\cos\psi_{s_c}} = \cdots$$

$$= \frac{\rho_r T_{pulse,eff}\beta_{swath,eff}}{k_0\cos\psi_{s_c}} = \frac{\Delta r K_a T_{pulse,eff}\beta_{swath,eff}}{k_0\cos\psi_{s_c}} = \cdots$$

$$= \frac{\Delta r K_a N_{fast}\beta_{swath,eff}}{k_0\,\Delta f_{\mathrm{ADC}}\cos\psi_{s_c}} = \frac{\Delta r N_{FFT}\beta_{swath,eff}}{\Delta f_{\mathrm{ADC}}\cos\psi_{s_c}} = \cdots$$

$$R_{swath_{pixlim}} = \Delta r_{gnd} N_{FFT} K_r, \quad (22)$$

where Δr_{gnd} is the ground range pixel spacing,

$$\Delta r_{gnd} = \frac{\Delta r}{\cos\psi_{s_c}}, \quad (23)$$

and K_r is a constant representing:

$$K_r = \frac{\beta_{swath,eff}}{\Delta f_{\mathrm{ADC}}} = \frac{\eta_{IF}\beta_{IF}}{\Delta f_{\mathrm{ADC}}}. \quad (24)$$

Therefore, the ground range pixel-limited swath is essentially the product of the number of FFT samples taken from the ADC output of the truncated IF filter and the ground range pixel spacing.

As mentioned, the final limited ground range swath will be the minimum of the pixel- and beam-limited swaths, i.e.

$$R_{swath_{lim}} = \min\left\{\begin{matrix} R_{s_c}\sin\left(\frac{\theta_{EL_{3dB}}}{2}\right)\left[\frac{1}{\sin\left(\psi_{s_c}+\frac{\theta_{EL_{3dB}}}{2}\right)} + \frac{1}{\sin\left(\psi_{s_c}-\frac{\theta_{EL_{3dB}}}{2}\right)}\right], \\ \Delta r_{gnd} N_{FFT} K_r \end{matrix}\right\}. \quad (25)$$

As an aside, the ground range resolution follows a similar treatment to range swath and range pixel spacing and is given by:

$$\rho_{r\_gnd} = \frac{\rho_r}{\cos\psi_{s_c}}. \tag{26}$$

2.3. Squint Mode Cross-Range Swath

Unlike the range dimension, the squint mode cross-range swath is only beam-limited. The cross-range direction is defined perpendicular to the range direction and is dependent on the azimuth beamwidth of the antenna and the slant range at the squinted aperture center. The developments for beam-limited cross-range swath have the corresponding geometry shown in Figure 6.

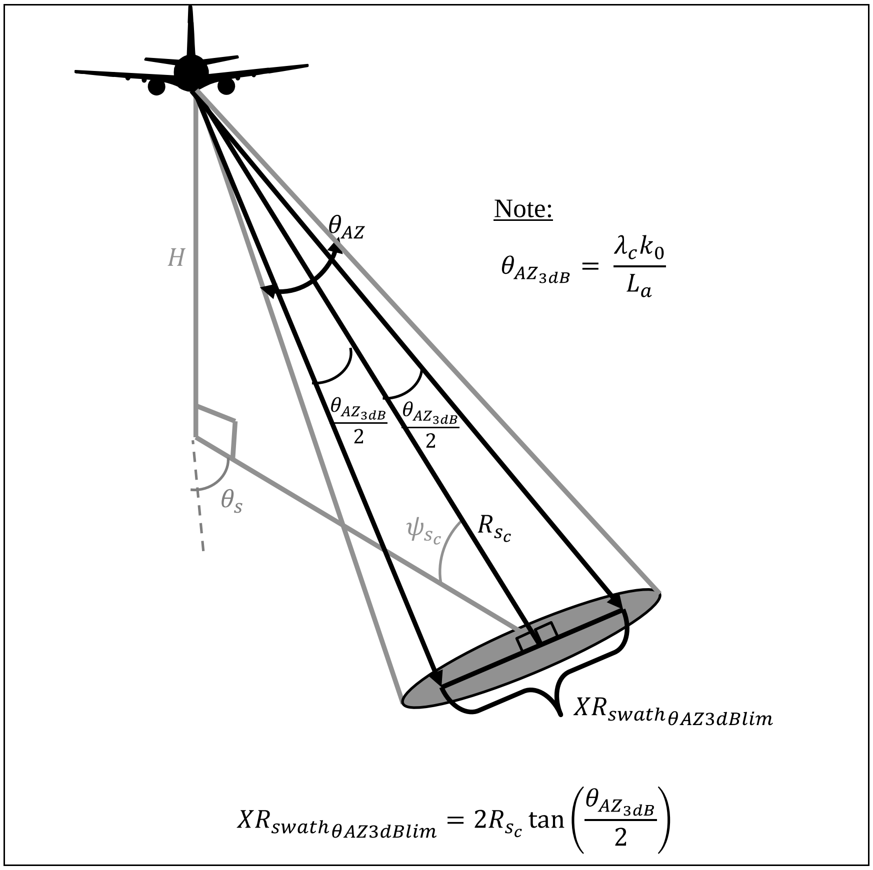

Figure 6. Beam-limited Cross-Range Swath

The 3-dB azimuth beamwidth of the antenna is given by the wavelength at the center frequency, λ_c, the physical length of the antenna in meters, L_a, and any windowing that may be applied to the illumination pattern:

$$\theta_{AZ_{3dB}} = \frac{\lambda_c k_0}{L_a} \tag{27}$$

The beam-limited cross-range swath entails the physical width covered by the antenna beamwidth footprint on the ground at the squinted aperture center. The cross-range swath is the same in the slant or ground plane.

Applying right triangle relationships, the 3-dB beam-limited cross-range swath is given at the slant range at the squinted aperture center as:

$$XR_{swath_{\theta AZ3dBlim}} = 2R_{s_c} \tan\left(\frac{\theta_{AZ_{3dB}}}{2}\right), \quad (28)$$

where $XR_{swath_{\theta AZ3dBlim}} \rightarrow \infty$ if $\theta_{AZ_{3dB}} \geq \pi$.

Note that the cross-range can be further constrained to the 3-dB beam-limit at the near slant range. This approach is a design choice to ensure that the near range edges of the patch are still illuminated by the 3-dB beamwidth of the antenna.

2.4. Squint Mode Synthetic Aperture Time

As mentioned, the synthetic aperture time will depend on the synthetic aperture length in meters, X_a, and platform ground speed in m/s, v_g, i.e.,

$$T_a = \frac{X_a}{v_g}. \quad (29)$$

This subsection describes the mathematics to find synthetic aperture time from these two parameters.

2.4.1. Synthetic Aperture Length

The synthetic aperture length depends on the ground range and squint angle at the squinted aperture center, as well as the ground synthetic aperture angle. The latter is given by the wavelength at the center frequency, λ_c, any windowing that may be applied to the IPR, and the desired azimuth resolution, ρ_a, projected onto the ground plane:

$$\theta_a = \frac{\lambda_c k_0}{2\rho_a \cos\psi_{s_c}}. \quad (30)$$

Finding the synthetic aperture length follows a formulation similar to that of range beam-limited swath. Figure 7 shows the geometry of interest for both a forward-looking and backward-looking squinted collect. Due to the squinted nature of the geometry, asymmetric near and far range aperture segments will compose the total synthetic aperture length,

$$X_a = X_{a_{near}} + X_{a_{far}}. \quad (31)$$

For the forward-looking collect, applying the law of sines and angle difference formula for sine yields:

$$X_{a_{near}} = \frac{R_{s_{c\_gnd}} \sin\left(\frac{\theta_a}{2}\right)}{\sin\left(\theta_s + \frac{\theta_a}{2}\right)}, \text{ and} \tag{32}$$

$$X_{a_{far}} = \frac{R_{s_{c\_gnd}} \sin\left(\frac{\theta_a}{2}\right)}{\sin\left(\theta_s - \frac{\theta_a}{2}\right)}. \tag{33}$$

For the backward-looking collect, the above equations are reversed. That is, $X_{a_{near}}'$ is given by Equation 33 and $X_{a_{far}}'$ is given by Equation 32. Thus the total synthetic aperture length for a forward- or backward-looking collect is:

$$X_a = R_{s_{c\_gnd}} \sin\left(\frac{\theta_a}{2}\right)\left[\frac{1}{\sin\left(\theta_s + \frac{\theta_a}{2}\right)} + \frac{1}{\sin\left(\theta_s - \frac{\theta_a}{2}\right)}\right], \tag{34}$$

where $X_a \to \infty$ if $\theta_s \leq \frac{\theta_a}{2}$.

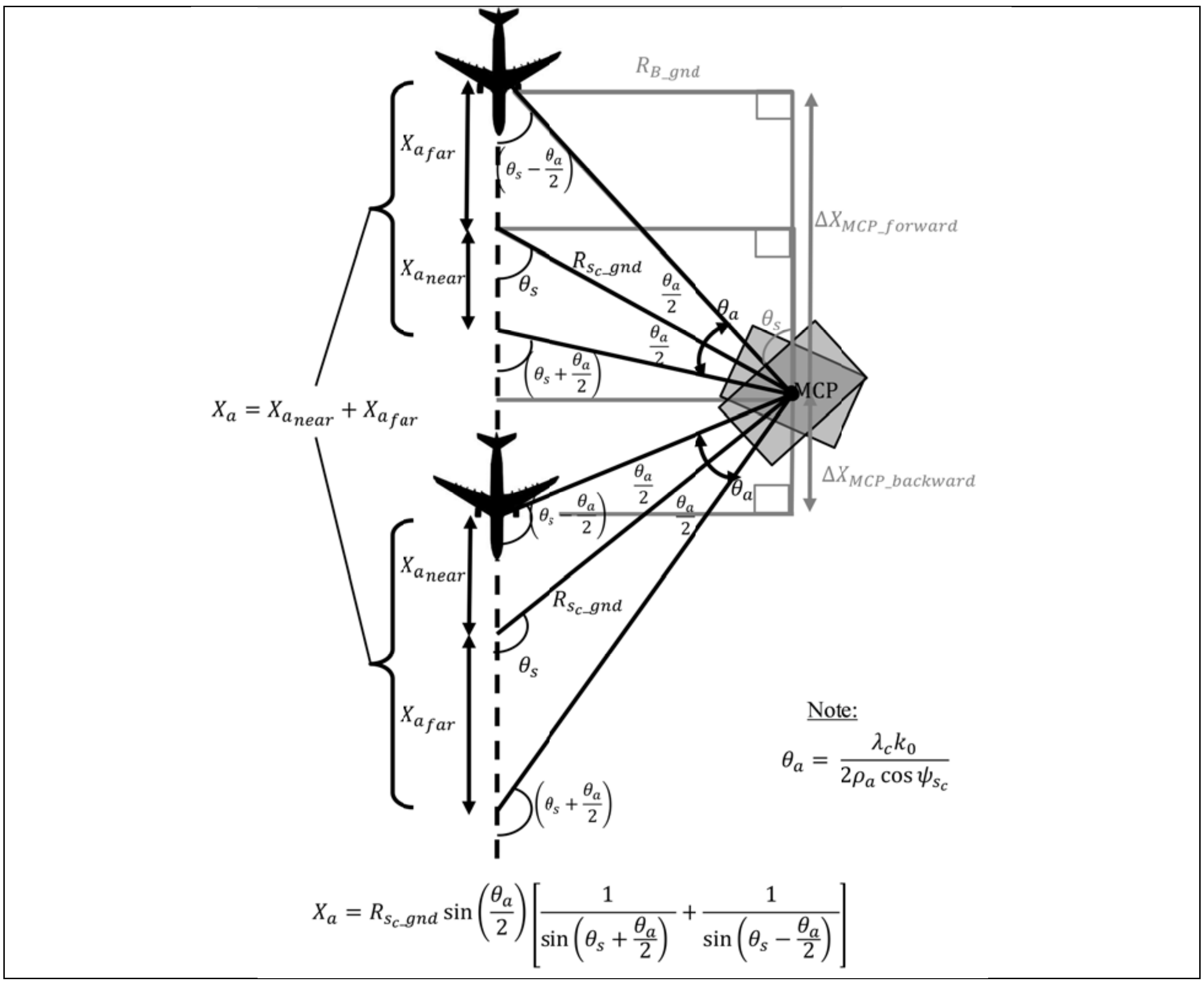

Figure 7. Synthetic Aperture Length

With some foresight, we compute the distance from the motion compensation point (MCP) which is roughly the patch center to the aperture start location of the radar next. This information will prove useful when looking at multiple patches in a trajectory.

For the forward-looking collect, we note from Figure 7 that this value is a positive shift given by:

$$\Delta X_{MCP\_forward} = X_{a_{far}} + R_{s_{c\_gnd}} \cos\theta_s.$$

For the backward-looking collect, the shift is negative and given by:

$$\Delta X_{MCP\_backward} = -X'_{a_{near}} - R_{s_{c\_gnd}} \cos\theta_s,$$

where the prime is a reminder that the backward-looking near range segment is given by Equation 33. In short, the absolute shift in the distance of the MCP to the aperture start, regardless of whether the radar is squinting forward or backward, is given by substitution as:

$$\Delta X_{MCP} = R_{s_{c\_gnd}} \left| \frac{\sin\left(\frac{\theta_a}{2}\right)}{\sin\left(\theta_s - \frac{\theta_a}{2}\right)} + \cos\theta_s \right|, \tag{35}$$

where $\Delta X_{MCP} \to \infty$ if $\theta_s \leq \frac{\theta_a}{2}$.

2.4.2. Platform Ground Speed

The platform ground speed is the vector result of the impact of wind speed and direction on the true air speed and direction of the platform. If ambient conditions are calm, the platform true air speed is the ground speed. However, if ambient conditions are not calm, aircraft must crab their true air speed direction if a specific ground speed direction is desired. Figure 8 shows the geometry and parameter relationships of such a scenario using right triangle properties. The resultant platform ground speed is:

$$v_g = \sqrt{{v_{TAS}}^2 - (w\sin\theta_w)^2} - w\cos\theta_w, \tag{36}$$

where v_{TAS} is the true air speed, w is the wind speed, and θ_w is the wind direction relative to the platform.

In short, the synthetic aperture time, by substitution of the platform ground speed and synthetic aperture length, is:

$$T_a = \frac{R_{s_{c\_gnd}} \sin\left(\frac{\theta_a}{2}\right)\left[\frac{1}{\sin\left(\theta_s + \frac{\theta_a}{2}\right)} + \frac{1}{\sin\left(\theta_s - \frac{\theta_a}{2}\right)}\right]}{\sqrt{{v_{TAS}}^2 - (w\sin\theta_w)^2} - w\cos\theta_w}, \tag{37}$$

where $T_a \to \infty$ if $\theta_s \leq \frac{\theta_a}{2}$.

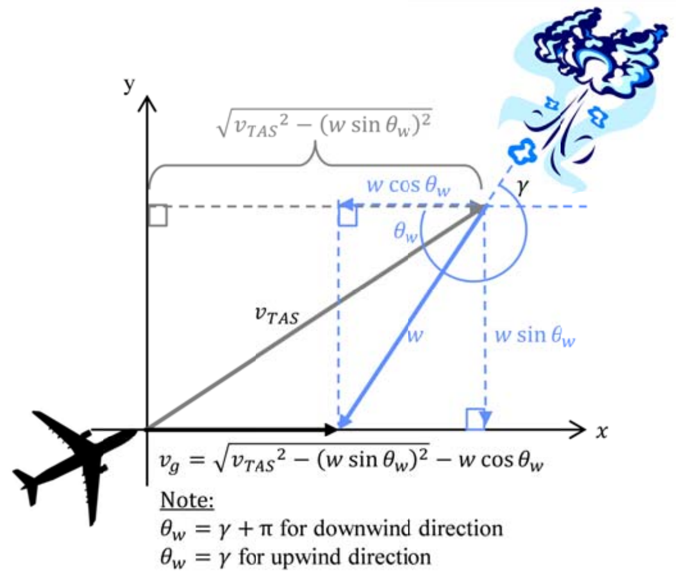

Symbol	Units	Description
v_{TAS}	m/s	Platform true air speed
w	m/s	Wind speed
γ	radians	Wind direction
θ_w	radians	Wind direction relative to platform
v_g	m/s	Platform ground speed including wind

Figure 8. Platform Ground Speed

As an aside, understanding global wind speed and direction characteristics is important in being able to estimate reasonable SAR model results due to wind phenomenology. A radiosonde is generally an instrumented weather balloon that measures geopotential height, temperature, dewpoint depression, wind speed and direction, and pressure during its ascent and radios results to a launch station until it bursts. Wind speed and direction is often measured or interpolated to standard pressure levels with radiosonde devices at established stations worldwide twice a day at 00 and 12 Greenwich Mean Time (GMT). The Integrated Global Radiosonde Archive (IGRA) freely available through the National Climatic Data Center (NCDC) of the National Oceanographic and Atmospheric Administration (NOAA) provides global radiosonde data from 1940 through the present. Data for each sounding time and location is provided, as available, as well as monthly mean values for the station, month, time, and pressure level as long as at least 10 measurements exist. Statistics and distributions of global monthly average wind speed and direction from the IGRA are examined in Figure 9 for 1,380 radiosonde stations over the entire historical record and both 00 and 12 GMT launchings for 10 to 1000 hPa standard pressure levels, totaling 9,849,150 samples of data. The standard pressure level bounds correspond to mean sea level altitudes of 31,055 to 111 m (since pressure decreases with increasing altitude), which encompass the typical airborne platform above ground level altitudes we might expect for SAR applications.

From 1970 onwards, the IGRA data record is fairly uniform in terms of the number of samples per year. Global radiosonde stations and reporting were still being established before then. The wind direction is predominantly from about 90 degrees (blowing north- through south-east to west) and secondarily from about 270 degrees (blowing north- through south-west to east). These directional trends agree with climatic knowledge about prevailing winds on the earth. Unfortunately, many SAR applications do not guarantee imaging in a particular direction relative to the wind. We therefore assume for modeling purposes in this study that the wind directional probability relative to the platform is uniform.

Statistics	PDF	CDF
Wind Speed Mean: 22 knots Std. Dev.: 19 knots Median: 16 knots 90% Confidence: 2 to 59 knots Range: 0 to 254 knots	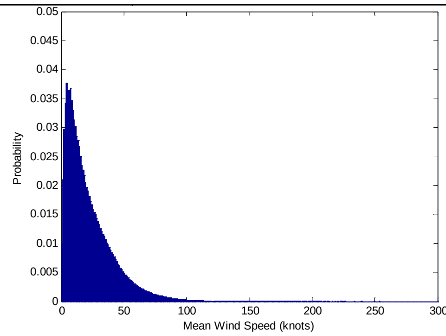	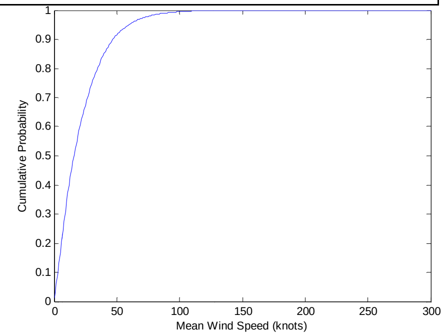
Wind Direction Mean: 134 degrees Std. Dev.: 82 degrees Median: 99 degrees 90% Confidence: 44 to 292 degrees Range: 0 to 360 degrees	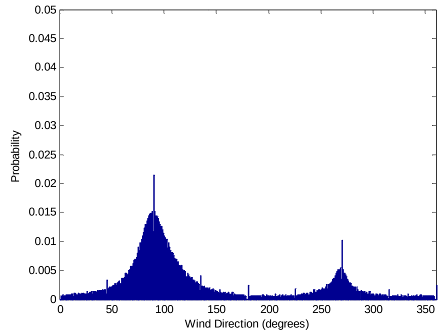	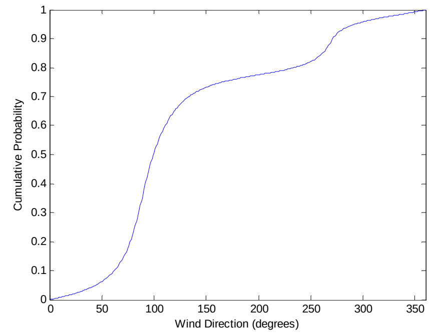
Date Coverage (9,849,150 samples) Mean: 1989 Std. Dev.: 15 years Median: 1990 90% Confidence: 1964 to 2011 Range: 1940 to 2014	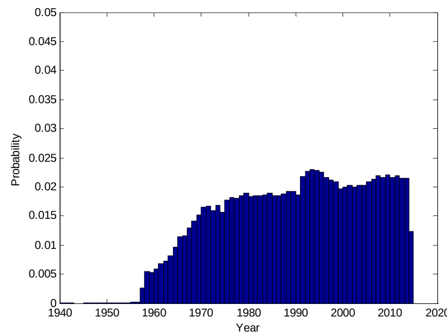	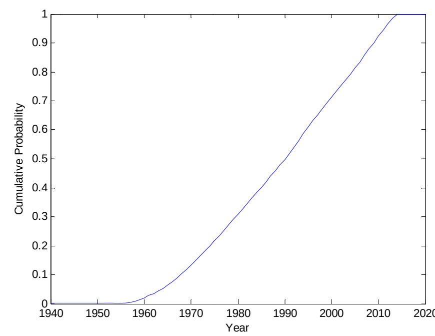

Radiosonde Station Locations

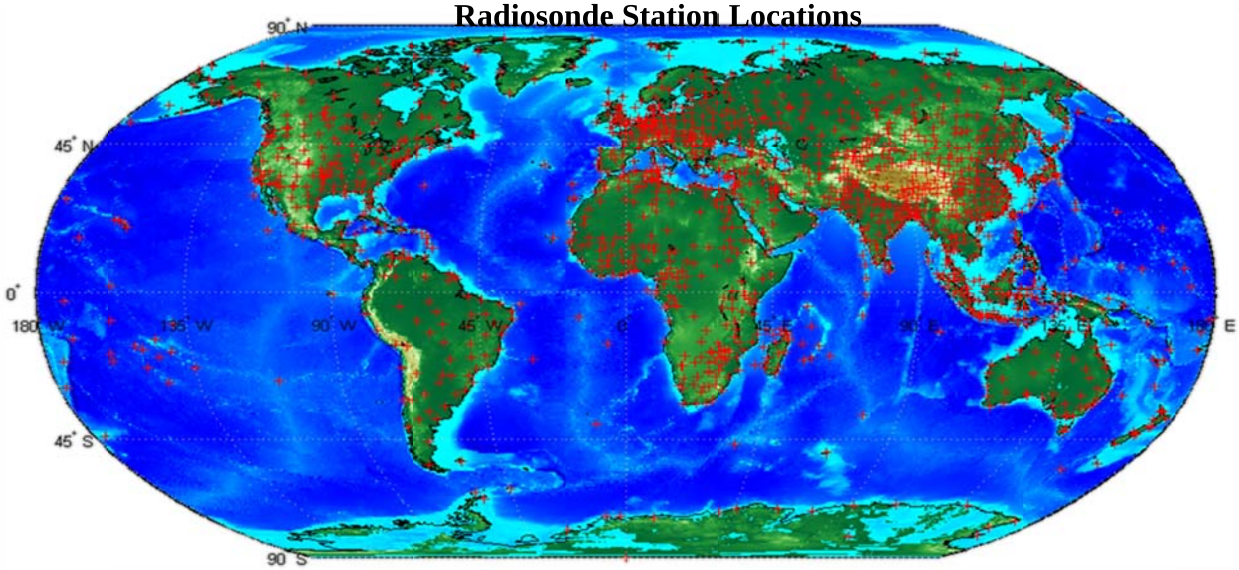

Figure 9. Wind Characteristics Based on Monthly Averages from 10 to 1000 hPa Standard Pressure Levels at 00 and 12 GMT for 1,380 Radiosonde Stations Worldwide

The global average monthly wind speed can range from 0 to 254 knots but will be below 60 knots at the 95th percentile and has a median likelihood of being 16 knots. Wind speeds may exhibit higher or lower instantaneous values or local trends due to the influence of geographic location, season, time of day, and other climatic deviations. Wind speed bounds of 0 to 60 knots, or approximately the 90% confidence interval, are recommended for SAR performance modeling. However, we will assume bounds of 0 to 30 knots in this study to accommodate a slow-moving radar platform defined in Table 1 in the Appendix with a true air speed of 60 knots, which represents worst-case platform advance rates. The likelihood of such an aircraft flying in more than 75th percentile, 30-knot winds is low. Furthermore, 60-knot winds would cause the plane to hang in mid-air when the wind and platform velocity are in equilibrium. Platform advance rates would be driven to zero in this case, which we intentionally avoid by lowering the bound to 30 knots.

2.5. Squint Mode Single Image ROA and ACR Expectations

From Equation 1, we know that the rate of advance of a single image by substitution of all parameters will be:

$$\dot{L} = \frac{2\left[\sqrt{v_{TAS}{}^2 - (w \sin\theta_w)^2} - w\cos\theta_w\right]\tan\left(\frac{\theta_{AZ_{3dB}}}{2}\right)}{\cos\psi_{s_c}\sin\left(\frac{\theta_a}{2}\right)\left[\frac{1}{\sin\left(\theta_s + \frac{\theta_a}{2}\right)} + \frac{1}{\sin\left(\theta_s - \frac{\theta_a}{2}\right)}\right]}, \tag{38}$$

where $\dot{L} \to \infty$ if $\theta_{AZ_{3dB}} \geq \pi$, $\dot{L} = 0$ if $\theta_s \leq \frac{\theta_a}{2}$, and $\dot{L}$ is undefined if both of the latter angular conditions are met.

The rate of advance is thus fundamentally dependent on wavelength, antenna physical length, azimuth resolution, squint angle at the aperture center, platform true air speed, wind speed and direction, and any windowing factors. For broadside geometries (i.e., $\theta_s = \frac{\pi}{2}$), calm conditions, and a small synthetic aperture angle and 3-dB antenna beamwidth, rate of advance simplifies to:

$$\dot{L_B} = \frac{v_{TAS}\theta_{AZ_{3dB}}}{\theta_a\cos\psi_{s_c}} = \frac{2v_{TAS}\rho_a}{L_a} = \ \ v_{TAS}, \tag{39}$$

indicating that the ROA is simply the platform velocity and therefore will increase with an increase in the platform velocity. This result makes sense, since the synthetic aperture angle is equal to the antenna beamwidth for broadside stripmap mode, yielding an azimuth resolution of half the antenna length.

Likewise, from Equation 2, we know that the area coverage rate of a single image by substitution of all parameters will be:

$$\dot{A} = \frac{2\left[\sqrt{v_{TAS}^2-(w\sin\theta_w)^2}-w\cos\theta_w\right]\tan\left(\frac{\theta_{AZ_{3dB}}}{2}\right)}{\cos\psi_{s_c}\sin\left(\frac{\theta_a}{2}\right)\left[\frac{1}{\sin\left(\theta_s+\frac{\theta_a}{2}\right)}+\frac{1}{\sin\left(\theta_s-\frac{\theta_a}{2}\right)}\right]} \min\left\{\begin{matrix} R_{s_c}\sin\left(\frac{\theta_{EL_{3dB}}}{2}\right)\left[\frac{1}{\sin\left(\psi_{s_c}+\frac{\theta_{EL_{3dB}}}{2}\right)}+\frac{1}{\sin\left(\psi_{s_c}-\frac{\theta_{EL_{3dB}}}{2}\right)}\right], \\ \Delta r_{gnd}N_{FFT}K_r \end{matrix}\right\}, \qquad (40)$$

where $\dot{A}\rightarrow\infty$ if $\theta_{AZ_{3dB}}\geq\pi$, $\dot{A}=0$ if $\theta_s\leq\frac{\theta_a}{2}$, and $\dot{A}$ is undefined if both of the latter angular conditions are met.

The area coverage rate is thus fundamentally dependent on wavelength, antenna physical size, azimuth resolution, received signal bandwidth and processing samples, platform height above ground level, nominal grazing angle at broadside, squint angle at the aperture center, platform true air speed, wind speed and direction, and any IF filter roll-off characteristics. For broadside geometries (i.e., $\theta_s=\frac{\pi}{2}$), calm conditions, and a small synthetic aperture angle and 3-dB antenna beamwidth compared to the grazing angle, area coverage rate simplifies to:

$$\dot{A_B} = v_{TAS}\min\left\{\frac{R_B\theta_{EL_{3dB}}}{\sin\psi_B}=\frac{H\lambda_c k_0}{W_a\sin^2\psi_B},\frac{ck_0}{2K_a\beta_{pulse,eff}\cos\psi_B}N_{FFT}K_r\right\}, \qquad (41)$$

indicating that the ACR increases with increasing platform velocity. For beam-limited conditions, ACR will also increase with platform height above ground level or slant range, grazing angle, and wavelength, and decreasing physical antenna width. For range-limited conditions, ACR will increase with decreasing signal bandwidth or ADC sampling rate and increasing grazing angle, FFT length or effective IF filter bandwidth of the received echoes of the range scene extent.

We demonstrate ROA and ACR behavior as a function of some of these parameters next using the radar parameter definitions in Table 1 in the Appendix. Square resolutions are assumed.

Figure 10 shows the relationship between ground range swath and squint angle, antenna size, grazing angle, and resolution. Range swath is beam-limited for narrow elevation beamwidth antennas (i.e. large antenna sizes), squint angles near broadside, high grazing angles, and coarse resolutions. Otherwise, range swath is pixel-limited. Beam-limitations decrease the range swath from about 100 m to 2.5 km for the example parameters. Grazing angles typical of airborne platforms (i.e. 10 to 40 degrees) give higher range swaths over steeper grazing angles. Resolutions below 8 inches are not as beam-limited as coarser resolutions and provide the most consistent swath coverage over all angles.

Figure 11 shows the relationship between cross-range swath and squint angle, antenna size, and grazing angle. Broader azimuth antenna beamwidths, shallow squint angles, and shallow grazing angles provide a large cross-range swath. However, cross-range swath tends to be fairly stable and below 2 km for most parameter combinations examined.

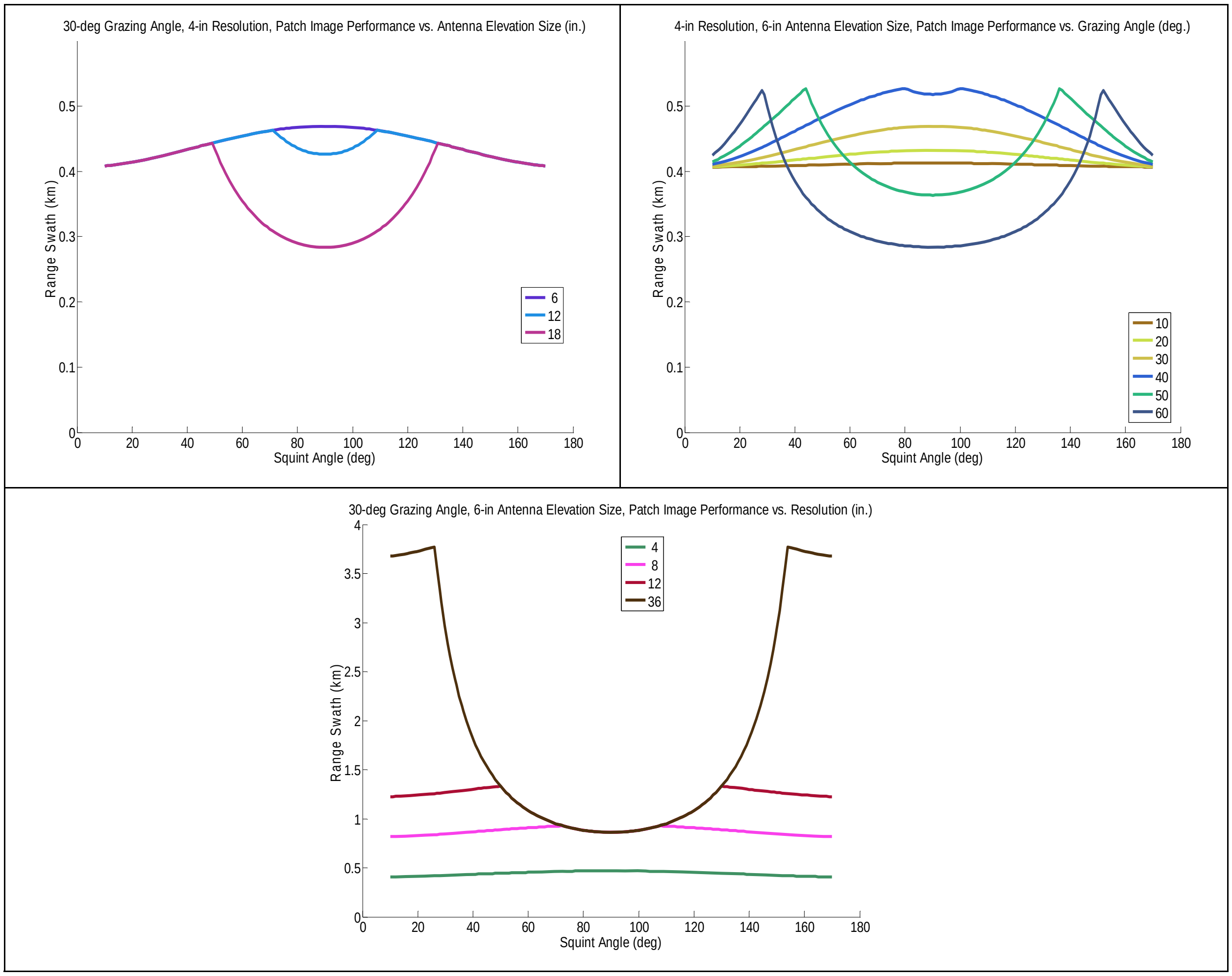

Figure 10. Ground Range Swath versus Squint Angle, Antenna Size, Grazing Angle, and Resolution

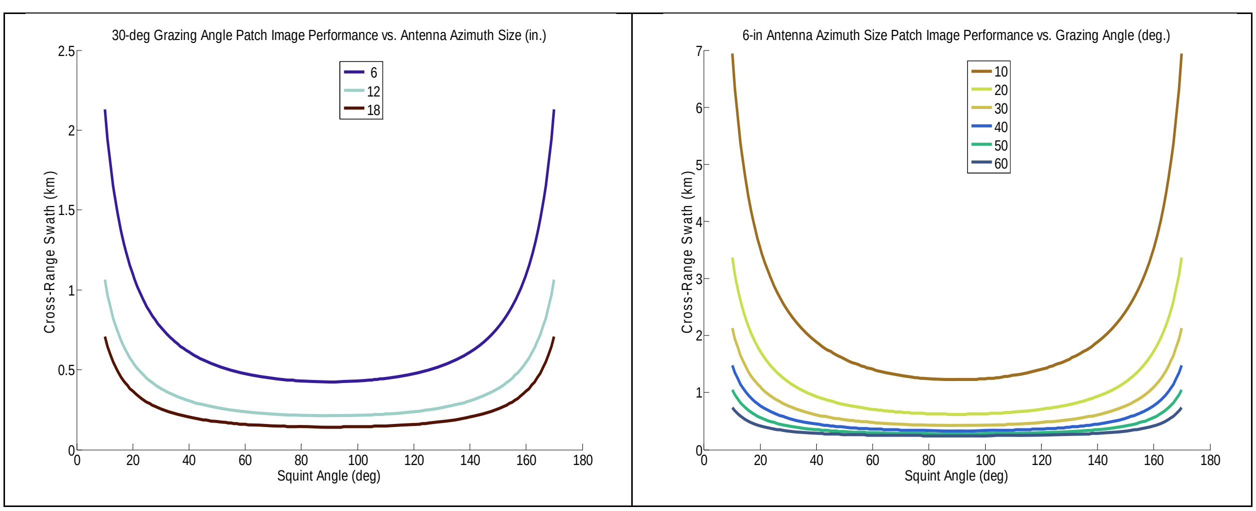

Figure 11. Cross-Range Swath versus Squint Angle, Antenna Size, and Grazing Angle

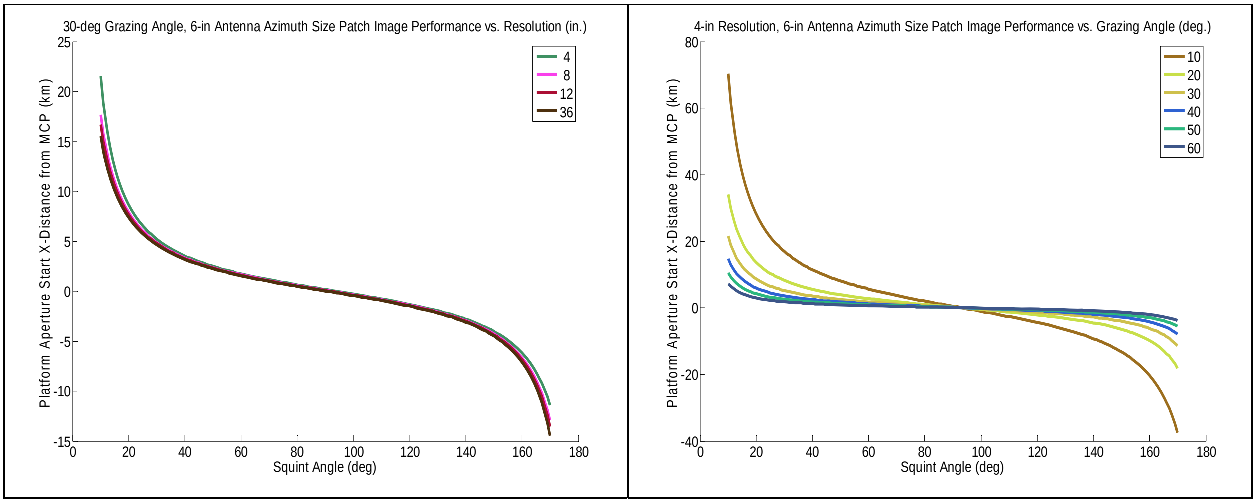

Figure 12. Distance from the MCP to the Aperture Start versus Squint Angle, Grazing Angle, and Resolution

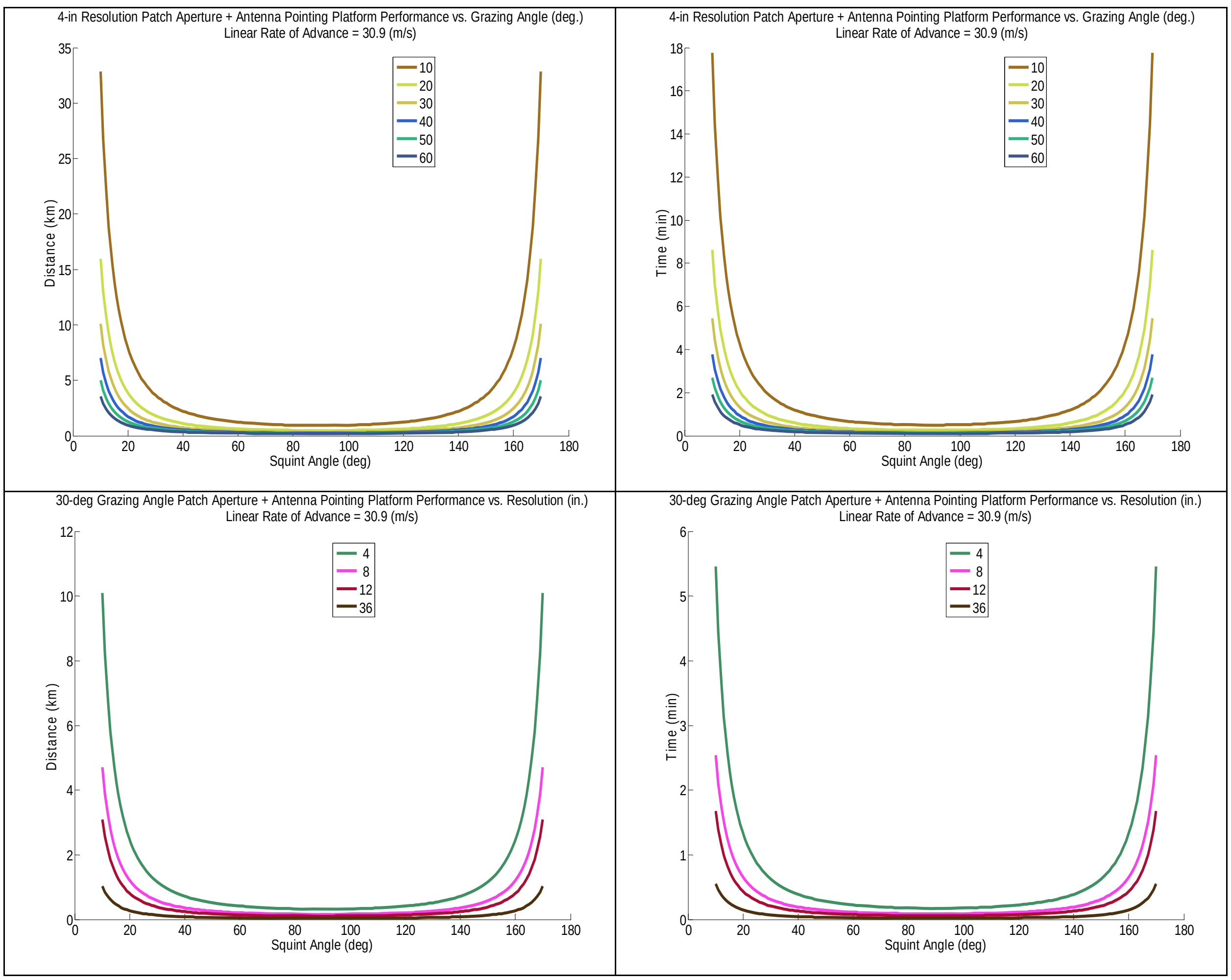

Figure 13. Synthetic Aperture Length and Time with Antenna Pointing Considerations versus Squint Angle, Grazing Angle, and Resolution

Figure 12 shows the relationship between the MCP distance from the aperture start location versus squint angle, grazing, and resolution. We note that shallower grazing angles and shallower squint angles require the most distance between the MCP and the start of the aperture. Forward-squinting fine resolutions and backward-squinting coarse resolutions require the most distance between the MCP and the start of the aperture as well. The distance between the MCP and aperture start location is asymmetric between forward- and backward-squinting imaging geometries because of the range and grazing angle variations for squinted geometries from aperture start to finish about the nominal range and grazing angle at aperture center. This distinction is on the order of several kilometers between broadside and squint mode imaging.

The platform rate of advance is a constant 30.9 m/s (i.e. 111 km/hr). We decidedly ignore plotting linear ROA, as it is merely the cross-range swath results of Figure 11 scaled by constants. Figure 13 shows the relationship between the synthetic aperture length and squint angle, grazing angle, and resolution. The synthetic aperture increases with shallow grazing angles and squint angles and finer resolution. The synthetic aperture length and time are generally below 2.5 km and 1 minute, respectively, for the example parameters.

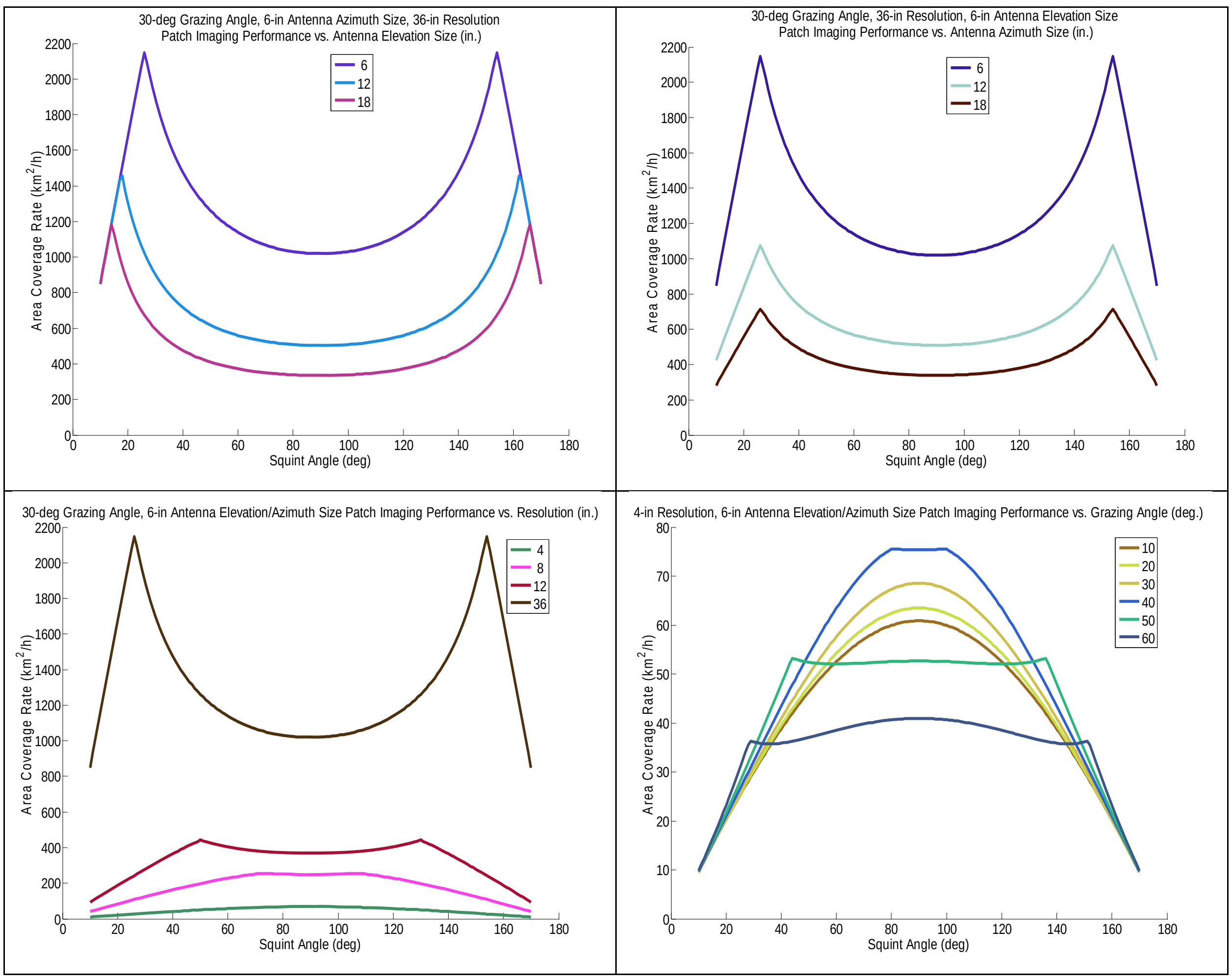

Figure 14. Area Coverage Rate versus Squint Angle, Antenna Size, Resolution, and Grazing Angle

Figure 14 shows the area coverage rate relationship to squint angle, antenna size, resolution, and grazing angle. Area coverage rate increases with broader antenna beamwidths in both elevation and azimuth, coarser resolution, and shallow-to-mid grazing angles. The range swath beam limitations are evident. Area coverage rates below 1100 km^2/hr are expected for most image patches with the examined parameters. Trajectory considerations will drive this amount far lower.

3. TRAJECTORY RATE OF ADVANCE AND AREA COVERAGE RATE THEORY

The previous chapter detailed rate of advance and area coverage rate theory for imaging a single patch. Ultimately, we do not desire to spotlight a single ground location but rather multiple ground locations. This chapter expands prior developments to understand linear rate of advance and area coverage rate for a trajectory.

3.1. Trajectory ROA and ACR Considerations

ROA and ACR for a trajectory require consideration of the following:

- Patch overlap to meet global positioning system (GPS) error variations in the true MCP and continuous coverage,
- Antenna pointing and settling time to the MCP for gimbaled systems prior to aperture start on a patch,
- Range of squint angles achievable with the antenna gimbal assembly,
- Optimum squint angle to meet the above and maximize ROA and ACR,
- Maximum segment length possible under squinted conditions above,
- Turnaround times when maximum segment length falls short of the desired segment length, and
- Hopping schemes that may decrease any required turnaround times to complete a desired segment trajectory.

GPS in the absence of selective availability and differential receivers can be expected to have up to about 15 m of error, but more commonly has less than 5 m of error. For the purposes of this study, we choose a patch overlap of 10 m to compensate for these error uncertainties.

Antenna pointing and settling time depends on the antenna gimbal assembly, and we choose 0.15 seconds for our study based on prior experience. Likewise, we keep to a range of squint angles between 45 and 135 degrees to avoid hitting gimbal stops and looking through non-ideal sections of the radome that may cause reflection or transmission losses that impact image quality.

Turnaround maneuvers may be necessary if the maximum segment length possible under squinted conditions falls short of the desired segment trajectory or if the synthetic aperture time at a given squint angle becomes longer than the turnaround time to reposition the aircraft to a different squint geometry with shorter synthetic aperture time. The latter case rarely occurs, whereas the former case is quite common for many radar parameters and geometries. A so-called "standard rate turn" or "rate one turn" for aircraft maneuvers involves turning at 3 degrees per second, which yields a 2-minute 360-degree turnaround time. For platforms that fly faster than 250 knots or about 129 m/s, a "half-rate turn" or 1.5 °/s for a 1-minute turnaround is possible. However, for slow platforms a "rate two turn" or 6 °/s for a 4-minute turnaround is necessary. For the purposes of this study, a straight-line flight path is assumed for the platform, and the worst-case rate two turn of 4-minutes is assumed if maneuvers become necessary for continuous imaging of a desired area, since the platform velocity of 60 knots is quite slow.

Turnaround maneuvers are a substantial time penalty to rate of advance and area coverage rate compared to synthetic aperture, antenna pointing, or aperture platform positioning times. In order to reduce the number of turnaround maneuvers during a mission, a hopping scheme may be considered. That is, if the maximum segment length possible under squinted conditions falls short of the desired segment trajectory, the platform can interleave the imaging of the shorter maximum segment length possible with segment lengths that are not imaged or skipped in order to reposition the platform to image a later segment rather than executing a turn. A turnaround is then executed at the end of the desired segment length, or the location where twice the travel time to reposition the platform to image the first area that was skipped over is less than that of having to execute a turnaround maneuver. Some turnaround maneuvers are avoided in this manner to generate time savings for rate of advance and area coverage rate. Hopping with squinted geometries is not always straightforward as the platform start position of the desired later segment to be imaged may occur prior to the platform position at the end of the former imaged segment. Multiple contiguous skipped segments may result in this case. For simplicity in this study, if hopping had to be executed with more than one turnaround to backfill multiple contiguous skipped segments over an area, then hopping was not performed at all and only turnaround maneuvers were executed.

The optimum squint angle, maximum segment length, and hopping benefits for a mission are analyzed parametrically in this study. In order to present a fair assessment of radar capabilities we redefine ROA and ACR from our single patch methods to instead be measured by a fixed coverage area requirement. This approach is driven by several reasons. The cross-range swath for squinted geometries is a poor method to determine the actual coverage of a segment because squinted patches are rotated relative to the straight-line platform trajectory and will change size depending on the squint angle. Establishing a minimum coverage area for these rotated patches is therefore necessary. Furthermore, although squinted patches may be larger than a required minimum coverage area, the image quality at the patch edges may be degraded to the extent that a maximum coverage area with guaranteed performance is desired. Factoring in patch overlap requirements further makes the performance determination of a radar configuration challenging for ROA and ACR since coverage area is actually taken away from the net result per patch.

Barring available fuel in an aircraft, the desired maximum segment length for a straight and level flight path will depend on the need to maneuver the platform. For example, this need may arise to accommodate a given application such as following a road or to reduce specific accumulated inertial measurement unit (IMU) errors. In particular, IMU heading error is an accumulated angular orientation error about the z-axis of the radar during straight and level flight with GPS-aided IMUs. This error leads to antenna pointing error or skewed illumination of the SAR scene based on where the antenna 3-dB beamwidth pattern is mistakenly assumed to be. Poor antenna pointing, or poor compensation of skewed illumination of the antenna pattern, corrupts SAR imagery with a noticeable intensity modulation across an image or between image patches. Heading error is often reduced by breaking off of the straight line path to perform S-turns or other maneuvers that change the horizontal-plane accelerations of the radar substantially to make the IMU errors measurable.

Figure 15a) shows the segment length distribution of 4,073 four-hour missions of an operational radar system imaging a road network with straight and level flight paths at broadside. The distribution of segment lengths is not Gaussian, with lengths no greater than 20 km and most below 12.5 km. Segment length limitations are based predominantly on the road network, although some biases exist in the data set due to the concept of operations. To eliminate any dependence on data set biases, we generalize that an ideal Gaussian-distributed segment length is probabilistically reasonable for most applications. The mean of 8.092 km and standard deviation of 2.987 km from the data set is assumed as a typical application straight and level flight segment distribution, with a 2σ range of 2.118 to 14.066 km.

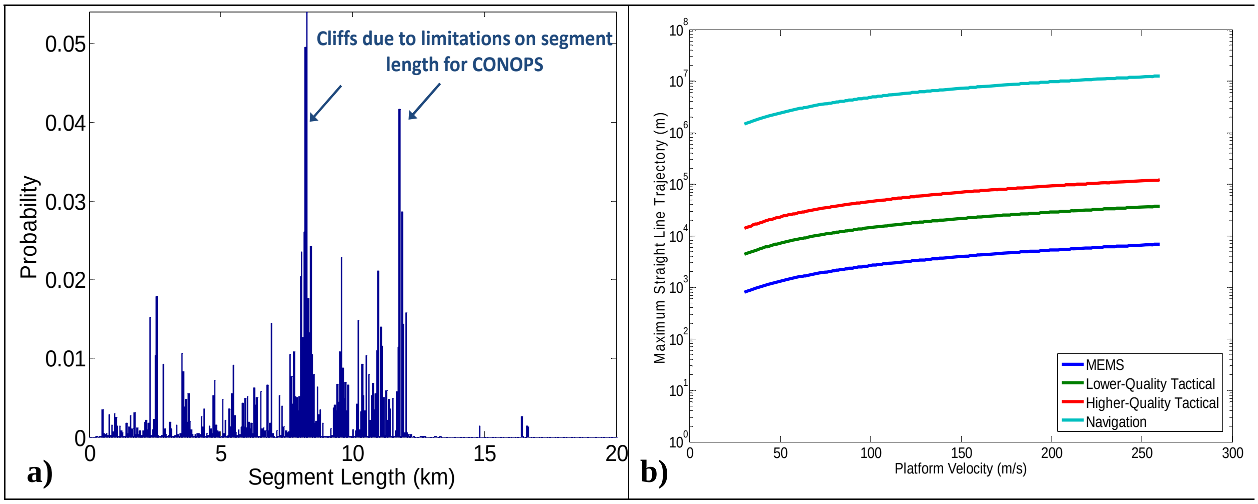

Figure 15. Maximum Segment Length Characteristics of a Straight and Level Flight Path SAR: a) Imaging a Road Network and, b) Breaking-off to Performing a Maneuver to Reduce Heading/Antenna-Pointing Error for Various Grade IMUs

Analysis of IMU heading error is rather involved and beyond the scope of this paper. We mere state here that anecdotal evidence suggests 0.03 beamwidths of antenna pattern misalignment yields about 1 dB of visible illumination variation in a SAR scene for the central 2/3 of the antenna beam. Anecdotal evidence also suggests that accumulated heading error beyond 70% of the desired antenna pointing error limit should be avoided. For a 6.8-degree 3-dB beamwidth antenna such as in Appendix A, this means 0.135 degrees of pointing error or 0.09 degrees of heading error should be avoided. A narrower beam antenna will have even stricter constraints.

Accumulation of heading error to the threshold cutoff will depend on platform velocity and IMU grade. More accurate IMUs and faster platforms will reach the heading error threshold more slowly. Based on select pessimistic specifications of various grade IMUs and the antenna in Appendix A, the maximum segment length to accumulate the threshold heading error is estimated in Figure 15b) for a range of SAR airborne platform velocities from slow unmanned aerial systems to jets. For a 60-knot platform velocity such as in Appendix A, the maximum segment lengths are 0.8, 4.4, 14.3, and 1,488.2 km for MEMS, lower- and higher-quality tactical, and navigation grade IMUs, respectively. Navigation grade IMUs are generally cost or size prohibitive for smaller, slower platforms. Thus, a higher-quality tactical grade IMU that causes maneuvers every 14.3 km or less to reduce heading error on a 60-knot platform is assumed reasonable for IMU-attributed maximum segment lengths. Experience dictates that IMU performance tends to exceed quoted specification performance but is obviously not guaranteed to do so. (S-turns may also be avoided using SAR-aiding techniques beyond the scope of this paper and for which the interested reader is referred to the literature [10].)

Based on analyses of maximum segment length for application- and IMU-driven constraints, we assume an absolute maximum desired segment length of 15 km in the following study. We also take the minimum segment width to be 450 m, which is consistent with the minimum coverage width of the road-imaging radar, fully cognizant that other applications may require a different (and usually larger) width. We further use the example radar parameter definitions, swath, and mission criteria of Table 1 in the Appendix unless parameter variations are explicitly stated.

3.2. Trajectory ROA and ACR Expectations

This section provides example analyses of trajectory rate of advance and area coverage rate expectations based on the considerations provided in the previous section. Example platform and imaging trajectories with patch layout at 4-inch resolution with a 6-inch square antenna are shown in Figure 16, Figure 17, and Figure 18 for broadside geometry, a squinted geometry with hopping, and a squinted geometry with only maneuvers, respectively. The imaging specifications are noted, as well as patch overlap, patch center, and platform start, middle, and end of aperture. The example broadside trajectory in Figure 16 was achieved without the need for any maneuvers (i.e. the unit segment is equivalent to the actual segment).

However, the squinted trajectory in Figure 17, which begins with a backward squint that is merely 5 degrees off broadside, requires hopping to complete the desired segment length. Hopping was achieved in this trajectory for the second, fourth, and (partial) sixth unit segments, which were completed on a turnaround pass. An immediate drop in area coverage rate from about 49 to 14 km^2/hr and linear rate of advance from about 110 to 31 km/hr is evident between the squinted and broadside results. The decrease is predominately due to the turnaround maneuver to backfill the hopped unit segments. Hopping is a consequence of the much smaller maximum segments with the backward squint, where maintaining patch overlap and forward progress of the platform implies increasingly longer apertures at shallower squint angles until a geometry cannot be found to meet the requirements. The rotation of image patches makes the achievement of patch overlap quite challenging and forces shallower squint angles with larger patch sizes. Unfortunately, the shallower squint angles come with increased synthetic apertures which drive even shallower squint angles until the geometry break-point.

The example squinted trajectory in Figure 18 further illustrates the penalty of squinted geometries and maneuvers on rate of advance and area coverage rate. Hopping was enabled but a straightforward scheme is not possible. The end of aperture of the first unit segment occurs after the start of aperture of the third unit segment, implying that two unit segments would have to be skipped to create a hopping scheme. This pattern continues between all odd-numbered segments. Since we do not consider multi-segment hopping schemes to maintain simplicity in this study, turnaround maneuvers are executed after each unit segment to image the next unit segment and the entire desired trajectory length, rather than executing turnaround passes to backfill multiple skipped unit segments. As a result of the maneuver-only squinted trajectory scheme, area coverage rate and linear rate of advance decrease to about 6 km^2/hr and 13 km/hr from the results of Figure 17 with only a 15-degree difference in the starting squint angle.

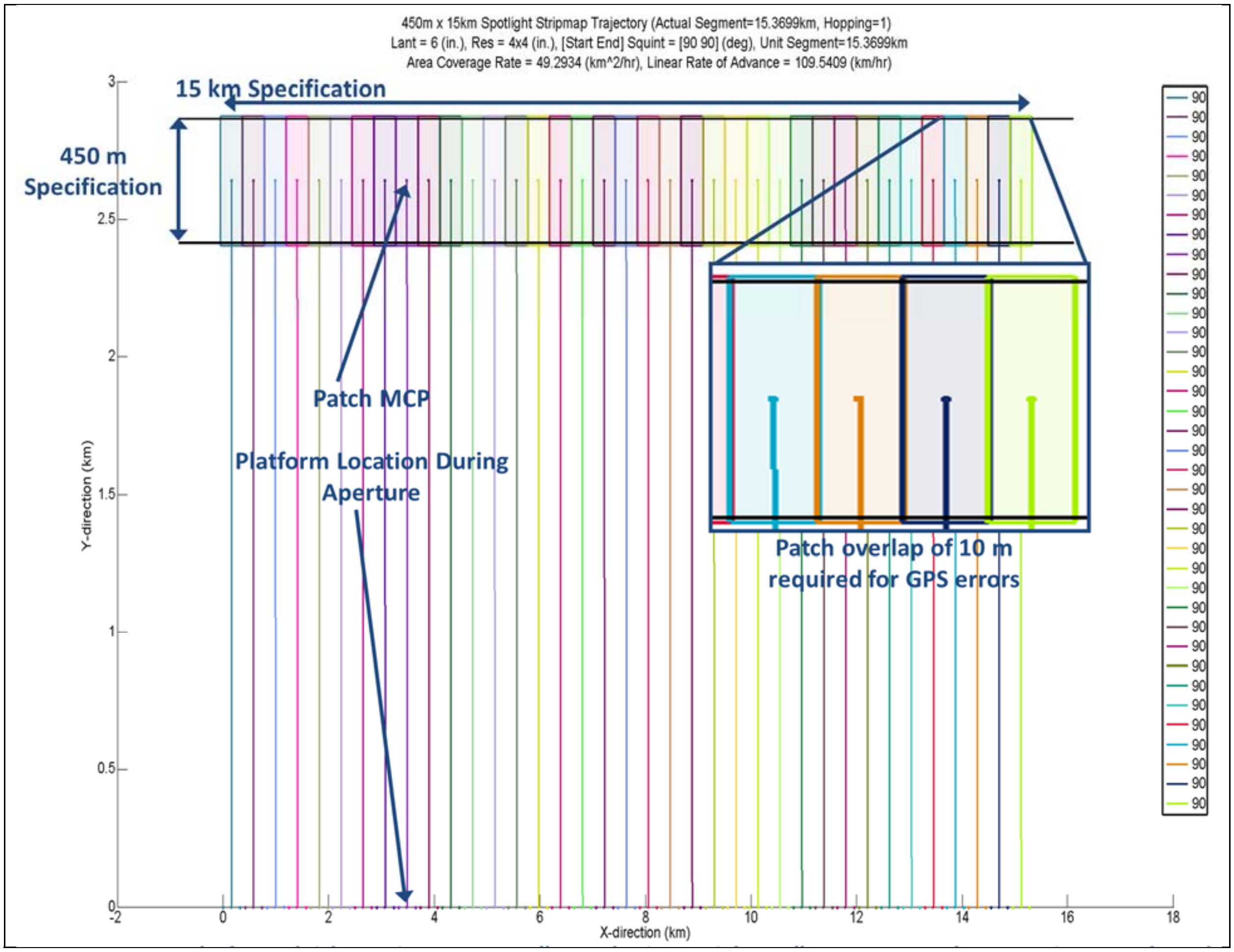

Figure 16. Example Broadside Trajectory at 4-inch Resolution with a 6-inch Antenna

A multi-segment hopping scheme would improve these results. However, ultimately any maneuvering, hopping or otherwise, versus being able to complete the desired trajectory in one pass quickly becomes unappealing for rate of advance and area coverage rate. We further observe that the larger squinted patch sizes do not add a great deal more meaningful coverage area to a scene beyond the specification width and length compared with the broadside case in order to counter the lost time of maneuvers and longer apertures.

Finally, one can observe from this and the prior example that there is no good reason to attempt to image a desired trajectory length with a backward-looking squint angle as the starting point for the given platform and radar parameters. Indeed, one would desire the starting squint angle to begin as forward-looking as possible in order to sweep to broadside or the backward-looking extreme. For the same antenna and resolution and, a starting squint angle of 45 degrees, one does observe great improvement in the area coverage rate and rate of advance to 42 km^2/hr and 93 km/hr. The squint angle sweep stabilizes close to broadside at 86-degrees, which balances the synthetic aperture platform advance and patch overlap requirements. Such a trajectory manages to do without hopping or other maneuvers but is still suboptimal to broadside due to the longer initial apertures until the stabilization squint angle is reached. A trajectory of only 86-degree squint angles still has slightly lower rates to the broadside case due to the slightly longer apertures.

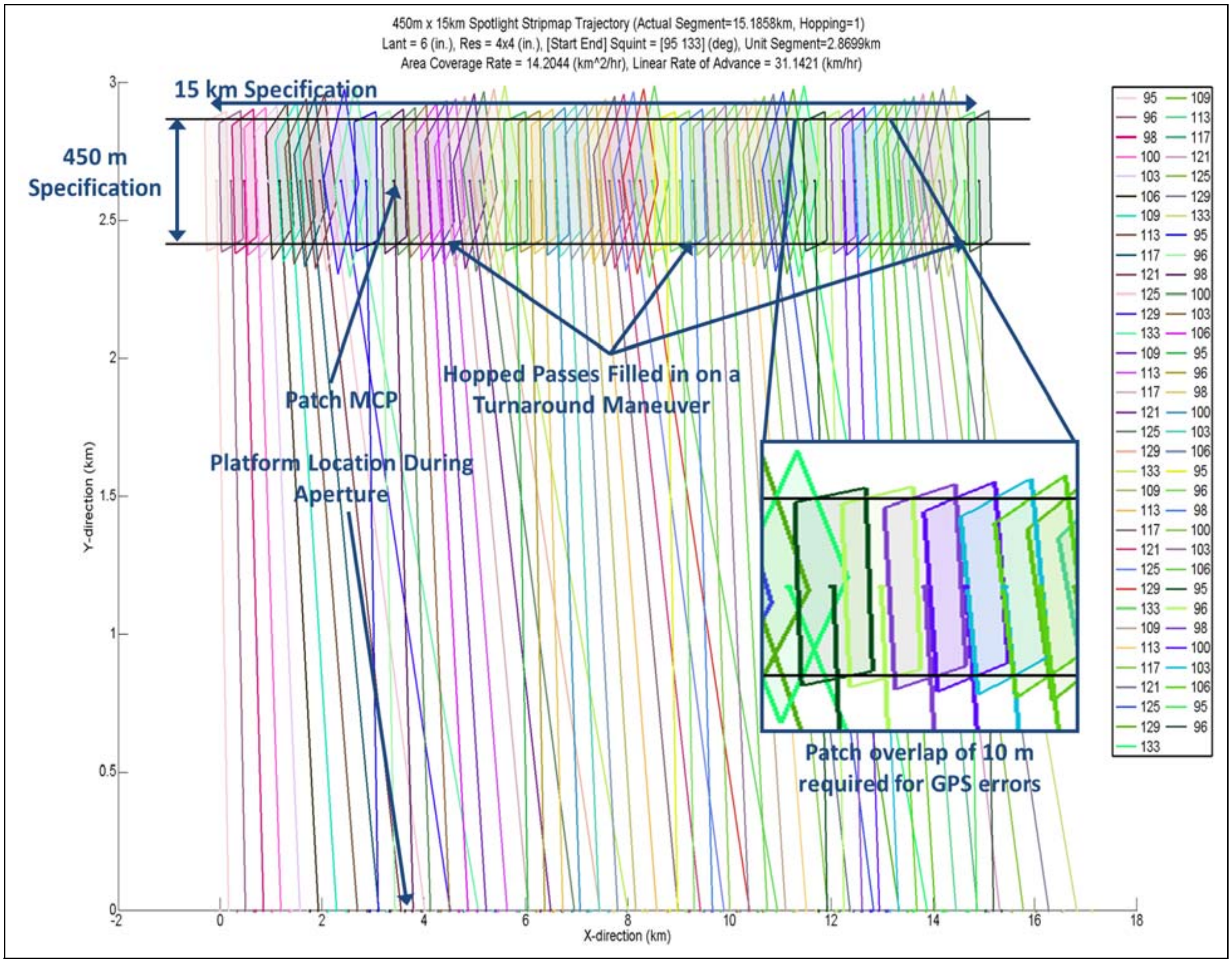

Figure 17. Example Squinted Trajectory at 4-inch Resolution with a 6-inch Antenna and Hopping

Squinted trajectories are never as ideal for area coverage rate and rate of advance as the broadside geometry based on the outlined cases. However, given a wide range of radar systems, the question arises if parameter changes to resolution, grazing angle, and antenna size coupled with a squinted trajectory might yield an improvement over broadside imaging. This question is examined in Figure 19 and Figure 20, which show rate of advance and area coverage rate as a function of the aforementioned parameters for broadside and squinted trajectories, respectively.

Rate of advance and area coverage rate results in Figure 19 indicate the following trends at broadside. Large azimuth size antennas cannot meet the desired segment length without maneuvers at fine resolutions, which plummet results compared to a 6-inch square antenna.

However, as resolution becomes coarser, larger (narrower azimuth beam) antennas provide comparable performance. For narrow elevation beam antennas, the 450-m range swath requirement is not met at broadside due to beamwidth limitations, which is corroborated by Figure 10 results. Furthermore, only grazing angles below 40 degrees for 6-inch square antennas are able to meet trajectory requirements. Finally, shallower grazing angles increase rate of advance and area coverage rate minimally as resolution becomes coarser.

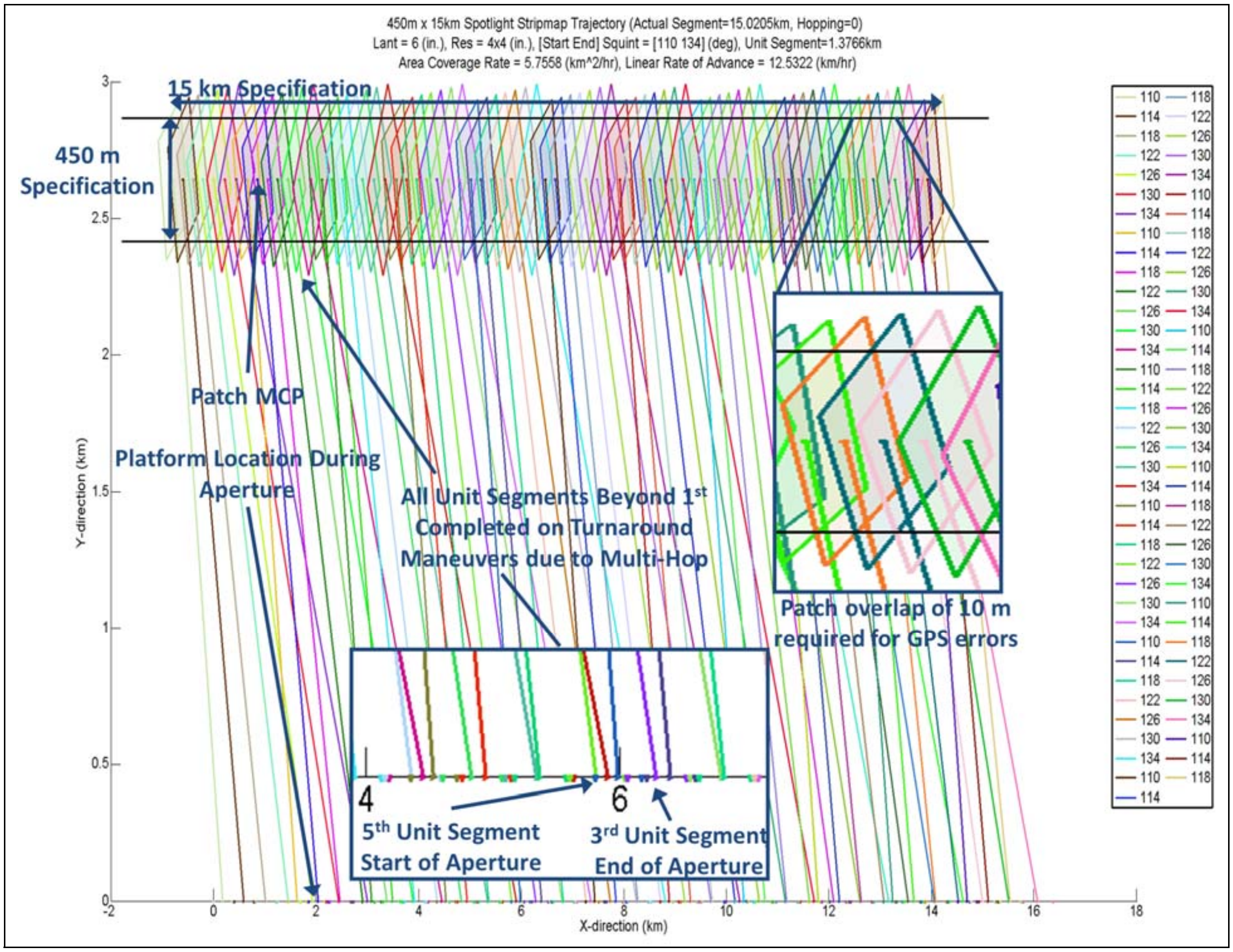

Figure 18. Example Squinted Trajectory at 4-inch Resolution with a 6-inch Antenna and Only Turnaround Maneuvers due to a Multi-Segment Hop Requirement

Figure 20 shows the following rate of advance and area coverage rate trends for the "optimum" or best-performing squinted trajectory for the given parameters. Narrow azimuth beam antennas have lower rate of advance and area coverage rate for the desired segment length at finer resolutions due to maneuvers, with comparable performance occurring as resolution becomes coarser. Rate of advance and area coverage rate decrease as antenna elevation size increases due to lower range swath coverage for the narrower beams. This effect is worse with finer resolutions but coarser resolutions also show a significant distinction. Rate of advance and area coverage rate decrease with increasing grazing angle overall and plateau as resolution coarsens.

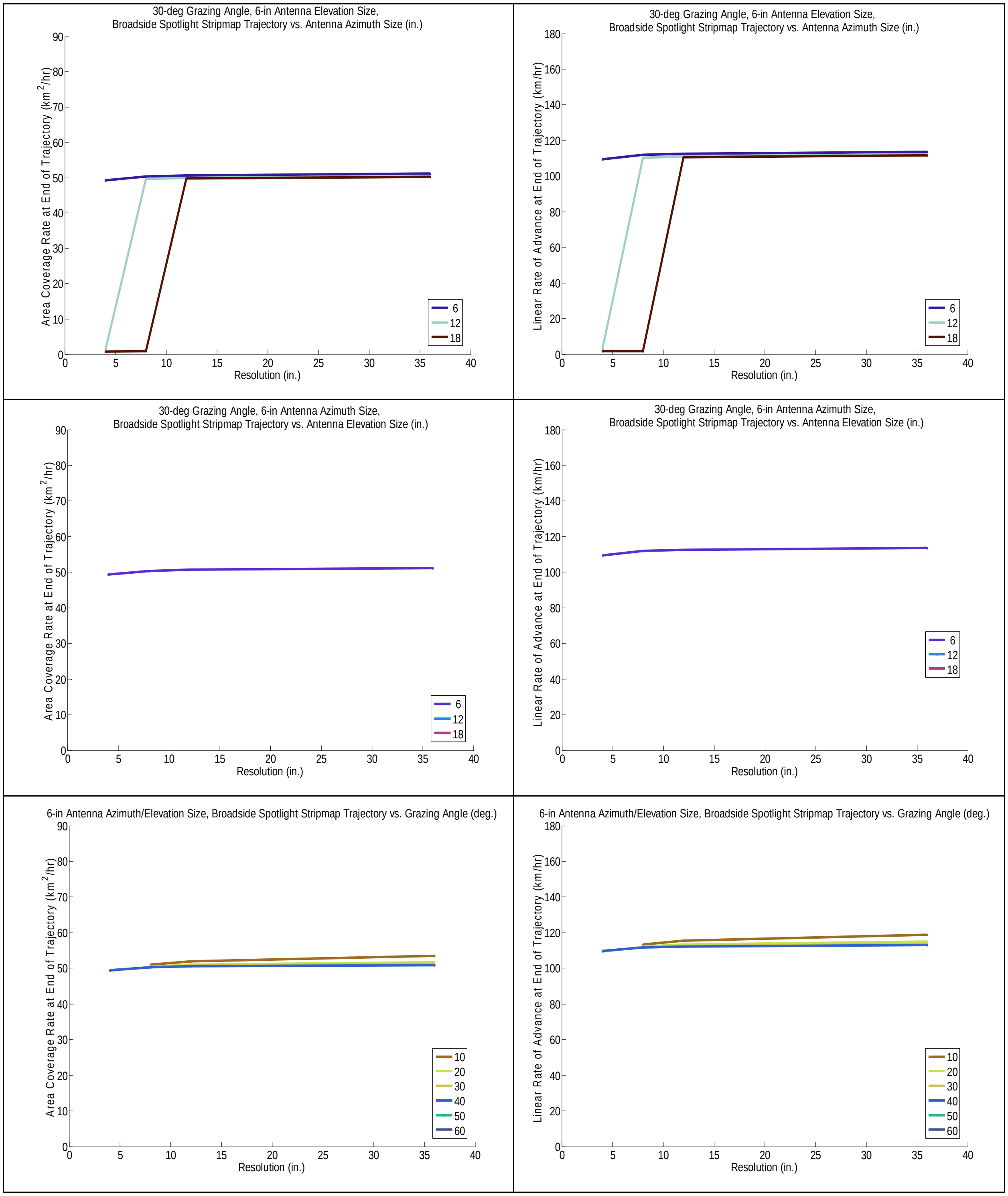

Figure 19. Broadside Spotlight Stripmap Trajectory Area Coverage Rate and Linear Rate of Advance vs. Resolution for Varying Antenna Dimensions and Grazing Angles Over a 15 km Coverage Distance

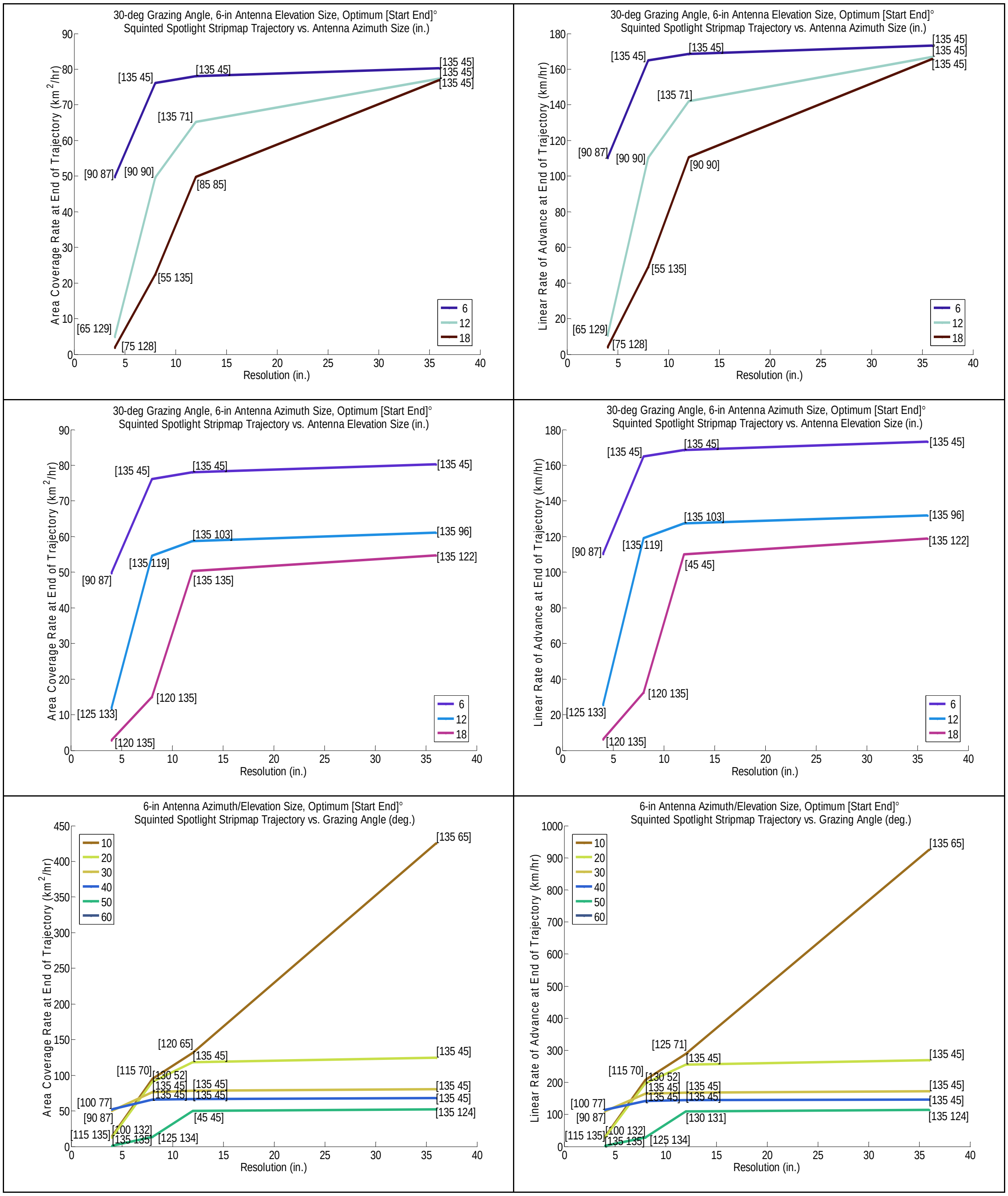

Figure 20. Squinted Spotlight Stripmap Trajectory Area Coverage Rate and Linear Rate of Advance vs. Resolution for Varying Antenna Dimensions and Grazing Angles Over a 15 km Coverage Distance

Figure 20 also shows that the optimum starting-to-ending squint angle sweep in a trajectory tends to stabilize to a backward-to-forward-looking 135-to-45-degree approach as resolution coarsens. This effect is due to the shorter aperture times afforded by coarse resolutions, which allow for faster imaging and scene coverage versus the platform advance rate. At finer resolutions and narrower antenna beamwidths this trend in the optimum squint angle sweep is not evident.

In comparing Figure 19 and Figure 20, we observe that for squinted trajectories, the instantaneous rate of advance and area coverage rate can be larger than the expected platform advance rate of about 111 km/hr and platform area coverage requirement of roughly 50 km^2/hr. The results merely imply that for short desired segment lengths, squinted geometries image larger areas faster than what the platform needs to move to complete the synthetic aperture at broadside. This result makes sense since at broadside, the radar images at the rate of the platform velocity but squint permits the platform to look ahead or backwards to image areas far beyond the platform location with some independence from the platform velocity. However, as the desired trajectory length increases, penalties of maneuvering for squint versus broadside geometries eventually drive results to convergence with the expected platform rates at broadside. This behavior is shown in Figure 21 for the 6-inch square antenna at 10-degree grazing angle and 4-inch square resolution size as a function of the starting squint angle. The 135-degree starting squint angle provides the slowest convergence to the typical broadside performance rates. The best performance at the 135-degree starting squint angle is for desired trajectory lengths below 20 km, and the knee of the curve that tends toward convergence occurs near 50 km.

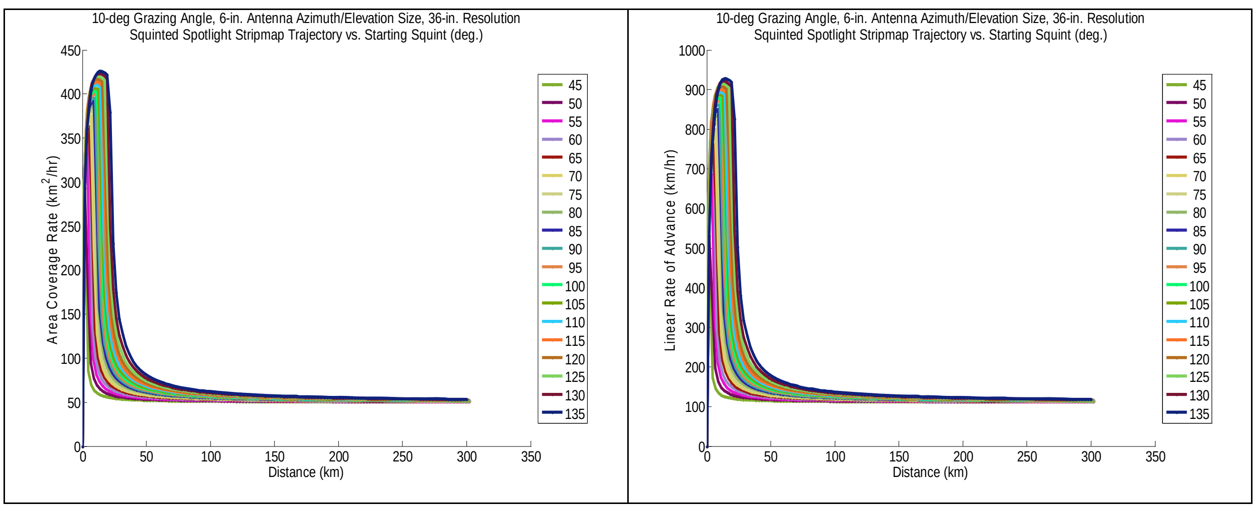

Figure 21. Squinted Spotlight Stripmap Trajectory Area Coverage Rate and Linear Rate of Advance vs. Covered Scene Distance for Starting Squint Angles at 10-degree Grazing and 36-inch Square Resolution for a 6-inch Square Antenna Size

We lastly observe that at 4-inch-square resolution for a 6-inch-square antenna, a near-broadside squint angle sweep from 90-to-87 degrees performs best in terms of rate of advance and area coverage rate versus other antenna size combinations and is only slightly different than the expected platform rates.

3.3. Mission ROA and ACR Expectations

In the prior section, we observed that squinted geometries for short desired trajectory lengths may out-perform broadside geometries in rate of advance and area coverage rate at coarse resolutions. However, the question that ultimately matters is whether an entire mission of many straight line trajectories might ever present favorable results for squinted versus broadside geometries and what the corresponding resolution, grazing angle, antenna size, and wind speed performance might look like. We investigate mission rate of advance and area coverage rate for a 4-hour mission next as a function of desired trajectory length up to the threshold of 15 km. A 100-trial Monte Carlo simulation of wind direction at a maximum speed of 30 knots is used for comparison to the case where no wind is present. The platform is assumed to turnaround and return to its point of origin within the mission time allotted.

Figure 22 shows the mission rate of advance and area coverage rate for a broadside geometry as a function of antenna size, grazing angle, and resolution. The 6-inch antenna azimuth size outperforms the 12- and 18-inch antennas in general but more so as the trajectory length increases from 1 to 15 km for a 6-inch elevation size antenna at 4-inch resolution and 30-degree grazing angle. As with a single trajectory, the entire mission has better performance with wider beam antennas in azimuth. As for the elevation dimension, only a 6-inch elevation antenna size works at 4-inch resolution with a 6-inch azimuth antenna size and grazing angle of 30-degrees to cover the desired swath. Since these results are similar to the 6x6-inch antenna results for varying azimuth antenna size, they are omitted. Performance as a function of resolution and grazing angle is fairly consistent for the 6-inch square antenna. These results also affirm prior trends for the single trajectory case at the mission level. Wind decreases performance overall as desired trajectory length increases for the 6-inch square antenna, showing up to about a 5 km/hr and 3 km^2/hr difference from no wind being present at 15 km. Higher winds would drive these results down further. Narrower azimuth beam antennas have such poor general performance that wind effects are negligible.

Figure 23 and Figure 24 show the mission rate of advance and area coverage rate for the optimum squinted geometry as a function of antenna size, resolution, and grazing angle. Wider beam antennas in both azimuth and elevation size have better performance as the desired trajectory length increases. A wider elevation beamwidth provides greater performance over a wider azimuth beamwidth due to the increase in range swath and rotated nature of squinted patches that provides greater coverage. Coarser resolutions perform better than finer resolutions as desired trajectory length increases due to the larger swath and shorter aperture times. The squint angle sweep occurring from 90 to 87 degrees for the 6-inch antenna at 4-inch resolution and 30-degree grazing angle is very close to the broadside case, indicating that a near-broadside trajectory performs best under the examined conditions. If the resolution is coarsened, however, a backward- to forward-looking sweep from 135 to 45 degrees performs best. Although performance increases with decreasing grazing angle at coarse resolutions, at 4-inch resolution the best performance is at 30 and 40 degrees, followed by 10 and 20 degrees. Wind decreases performance overall as the desired trajectory length increases. Finally, at the trajectory length of 15 km, mission rate of advance and area coverage rate performance trends do not flat-line, meaning applications and better grade IMUs that might tolerate longer trajectory lengths before executing maneuvers might benefit from even greater performance than outlined here.

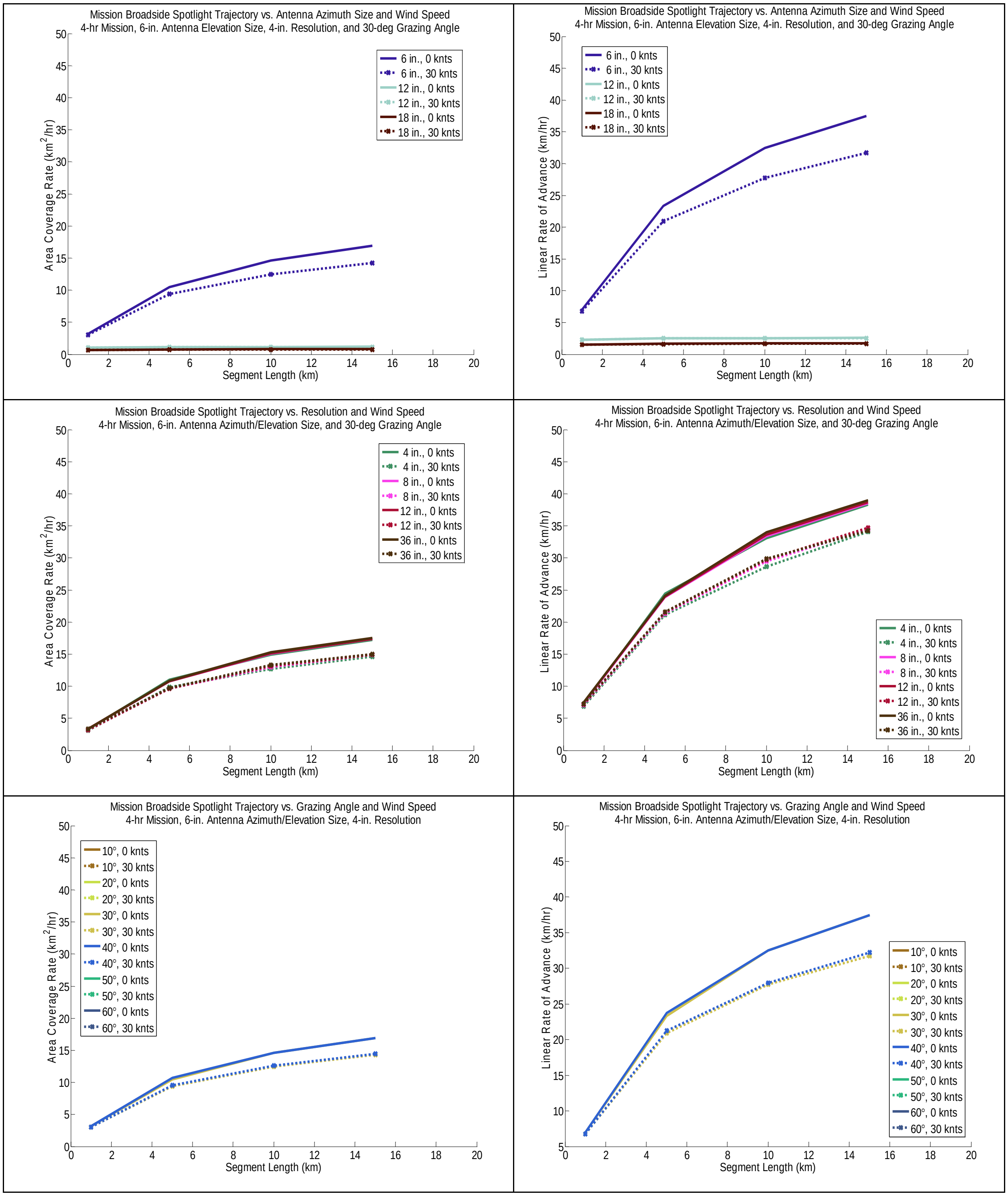

Figure 22. Broadside Geometry Total Mission Rate of Advance and Area Coverage Rate for a 4-hr Mission with Wind = [0, 30] knots as a Function of Antenna Size, Resolution, and Grazing Angle

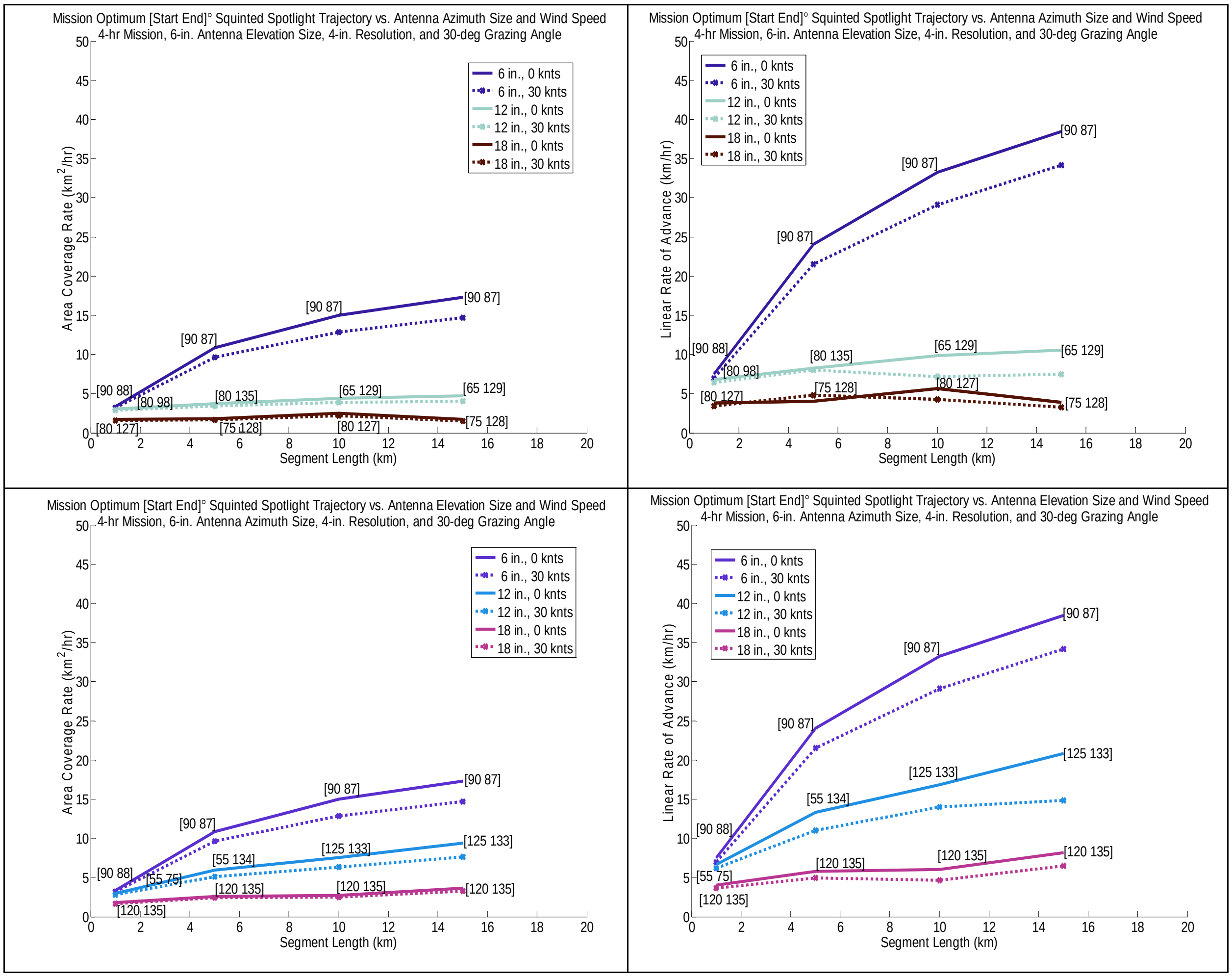

Figure 23. Squinted Geometry Total Mission Rate of Advance and Area Coverage Rate for a 4-hr Mission with Wind = [0, 30] knots as a Function of Antenna Size

For a short individual trajectory lengths, we observed that the linear rate of advance and area coverage rate could be instantaneously better than ideal platform and requirement values of 111 km/hr and 50 km^2/hr, respectively. Unfortunately, this perceived gain in rate of advance and area coverage rate is lost with maneuvers over an entire mission duration that includes coverage of multiple individual trajectory lengths with maneuvers between unit trajectories and a return to home base. Mission rates of advance and area coverage rates decrease to below 50 km/hr and 25 km^2/hr, respectively. Broadside geometry performance is difficult to beat with squinted geometries unless the resolution is coarse. Imaging mode or geometry considerations cannot compensate for the advantage of a wider beam antenna in both azimuth and elevation.

We finally note that application specifics matter when selecting system parameters. For example, coherent change detection applications rely on subtle phase differences between passes and overlapped patches to produce quality products. Shadows (i.e. low coherence areas) appear in the line-of-sight direction of the radar which changes with linear squinted trajectories per patch. Overlapped patch areas will have non-coincident shadows that will obscure more area and appear decorrelated, though not necessarily due to imagery changes of interest. Antenna alignment to image targets with limited angular extents may be more difficult for linear squinted trajectories as well. On the other hand, if large angular diversity is desired, a squinted pass has changing grazing and azimuth angles over the synthetic aperture. Coarser resolution may improve rate of advance and area coverage rate performance, but application suitability should be considered. Large targets may fair well at coarser resolutions but smaller targets may not, and objectives such as detection have less stringent requirements than identification, regardless of target size. Likewise, the backscatter of targets often varies with grazing angle, and a grazing angle that may optimize rate of advance or area coverage rate may not be ideal for detecting or analyzing the target. These system trades, along with others such as signal-to-noise ratio, are ever-present for the radar designer.

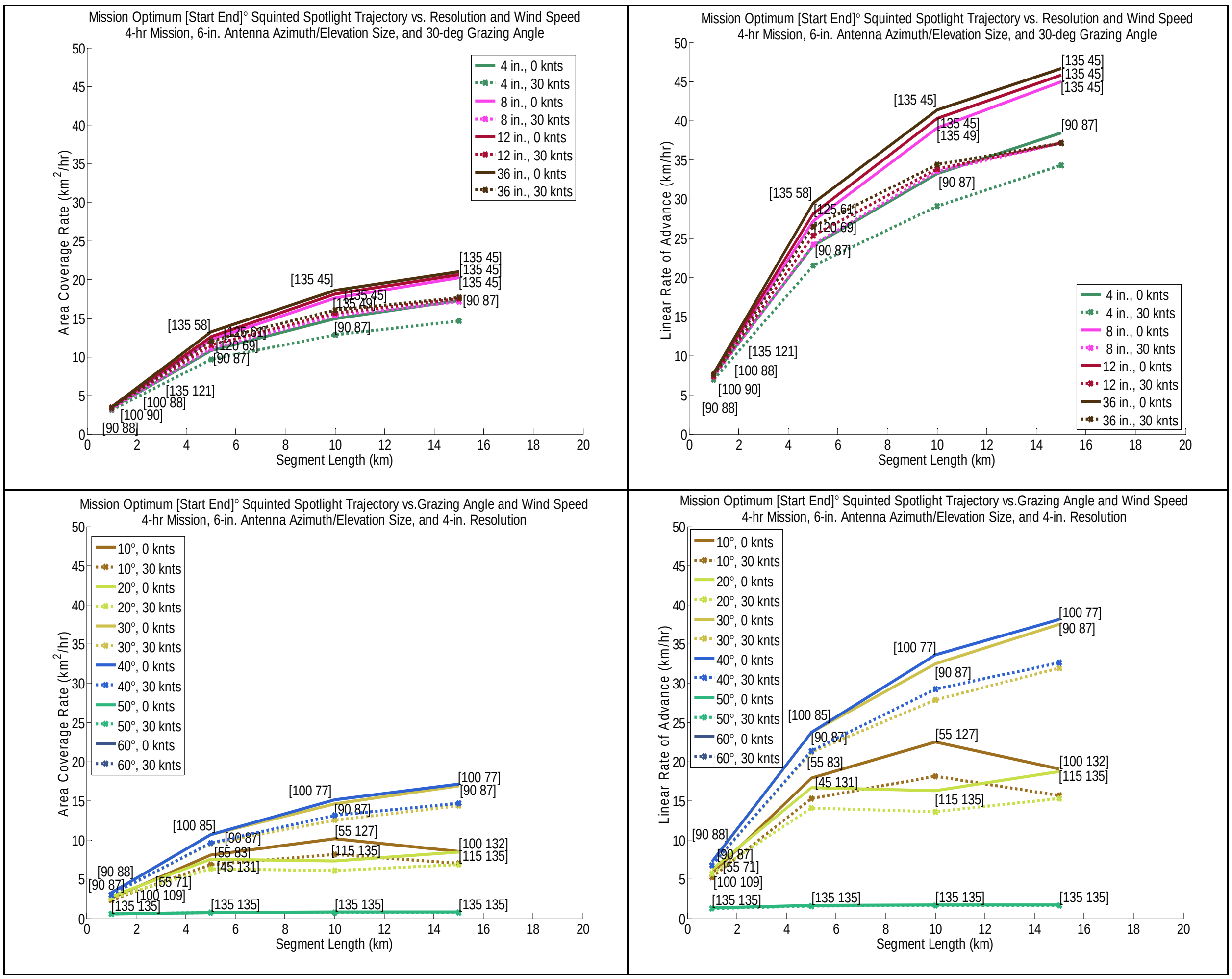

Figure 24. Squinted Geometry Total Mission Rate of Advance and Area Coverage Rate for a 4-hr Mission with Wind = [0, 30] knots as a Function of Resolution and Grazing Angle

4. CONCLUSIONS

This report has investigated the linear ground distance per unit time and ground area covered per unit time of producing synthetic aperture radar imagery, termed linear rate of advance (ROA) and area coverage rate (ACR). These metrics are important evaluations for platform and radar performance from an operational cost and limited resource standpoint, in addition to successful mission execution. A sensor that can provide greater mission (or multi-mission) performance per unit area per unit time (or ultimately operational dollar) is more cost-effective, more valuable as an ISR asset, and has more justifiable priority for use of limited resources.

Rate of advance and area coverage rate depend on many parameters of a SAR system such as wavelength, aircraft velocity, resolution, antenna beamwidth, imaging mode, and geometry. This report has detailed the mathematical theory behind area coverage rate and rate of advance for the general case of squinted geometries for the imaging of a single patch, including range beam- and pixel-limited swath considerations. Multi-patch linear segment and multi-segment mission performance has been examined for the varying parameter spaces of antenna size, resolution, grazing angle, squint angle, and aircraft ground velocity. Squinted geometry performance for a single short segment can instantaneously exceed ideal platform rate of advance and area coverage rates (which bound broadside performance) due to the ability to quickly sweep an area by mere antenna pointing as the platform advances at coarse resolutions. As the segment length increases, this gain is lost and convergence to the platform performance occurs. At fine resolutions such as 4-inches, a near-broadside imaging mode performs best due to the longer synthetic aperture lengths where large squint angle sweeps require hopping or maneuvering to keep up.

Maneuvers and wind are costly elements in rate of advance and area coverage rate performance, decreasing any instantaneous gain of a single segment to well below the ideal platform performance over the course of a mission. Maneuvers are difficult to avoid for linear trajectories due to accumulated heading errors of the inertial measurement unit and at times due to application requirements. These factors may impede more than 15 km of linear platform advance and can take a minimum of 1 to 4 minutes to execute. Over a 4-hour mission where a platform is assumed to return to home base, maneuvers done every 15 km more than halve the performance rates of a 60-knot platform. Global wind statistics suggest a median speed of 16 knots and 95th percentile below 60 knots, with preferential directions eastward and westward. A 30-knot wind drops mission performance of linear rate of advance and area coverage rate for a 60-knot platform by about 5 km/hr and 3 km^2/hr, respectively, while executing 15 km segments. Longer segment lengths within a mission are more afflicted by wind loss than shorter segments.

Not all combinations of radar or platform parameters are valid for executing specific coverage requirements of a mission. Narrow antenna beamwidths have less swath coverage and therefore struggle to outperform wider antenna beamwidths in rate of advance and area coverage rate unless coarse resolutions are desired. However, a broadside stripmap with a 6-inch antenna azimuth size requires the elevation antenna size to be 6-inches to meet a 450 m range swath requirement. For coarse resolutions, rate of advance and area coverage rate increase as a function of decreasing grazing angle due to a larger antenna spot size on the ground. If range swath requirements at broadside are 450 m, a 6-inch square antenna does not meet these specifications above 40-degree grazing. A similar specification for a squinted geometry implies keeping to grazing angles below 50 degrees, since rotated and overlapped patches of squinted geometries provide a little more coverage.

Finally, application specifics matter when selecting system parameters. Phenomenology, such as shadows and target backscatter, can change with grazing and azimuth angle. If angular variations in phenomenology within an image and between images are desired, a squinted trajectory may be quite valuable. However, if distinguishing subtle phase differences between overlapped patch edges or passes are desired, then broadside imaging may be more valuable. Furthermore, objectives on desired target types and analysis such as detection or identification often bound resolution. These system trades, along with others such as signal-to-noise ratio, should always be considered for a successful and cost-effective mission execution in addition to metrics such as rate of advance and area coverage rate.

5. BIBLIOGRAPHY

1. A. Freeman, et al., "The 'myth' of the minimum SAR antenna area constraint," *IEEE Transactions on Geoscience and Remote Sensing*, vol. 38, no. 1, pp. 320-324, Jan. 2000.

2. M. A. Richards, *Fundamentals of Radar Signal Processing*, McGraw Hill, New York, 2005.

3. D. P. Belcher and C. J. Baker, "High Resolution Processing of Hybrid Strip-map/spotlight mode SAR," *IEEE Proceedings on Radar, Sonar, and Navigation*, vol. 143, no. 6, pp. 366-374, Dec. 1996.

4. A. Freeman, "On Ambiguities in SAR Design," *EUSAR*, May 2006.

5. G. W. Davidson and I. Cumming, "Signal Properties of Spaceborne Squint-Mode SAR," *IEEE Transactions on Geoscience and Remote Sensing*, vol. 35, no. 3, May 1997.

6. A. W. Doerry and B. Marquette, "Radar Antenna Pointing for Optimized Signal to Noise Ratio," *Sandia National Laboratories Report*, SAND2012-10691, January 2013.

7. G. W. Stimson, *Introduction to Airborne Radar, 2nd Ed.*, SciTech Publishing, Inc., Raleigh, North Carolina, 1998.

8. D. L. Bickel, B. C. Brock, and C. T. Allen, "Spaceborne SAR Study: LDRD '92 Final Report," *Sandia National Laboratories Report*, SAND93-0731, March 1993.

9. "Integrated Global Radiosonde Archive," *National Climatic Data Center and National Oceanographic and Atmospheric Administration of the U.S. Department of Commerce*, http://www.ncdc.noaa.gov/oa/climate/igra/, accessed August 2014.

10. A. W. Doerry, "Estimating IMU Heading Error from SAR Images," *Sandia National Laboratories Report*, SAND2009-0183, March 2009.

There is no greater evil for men than the constraint of fortune.

- Sophocles

APPENDIX

Table 1. Example Radar, Platform, Ambient, and Area Coverage Parameters for ROA and ACR Computation

Symbol	*Units*	*Value*	*Description*
k_0	-	1.1822	3dB Taylor Window Impulse Response Broadening Factor
N_{FFT}	-	6000	Maximum Range FFT Size
K_r	-	0.8	Filter Bandwidth Factor to Prevent Roll-off Ambiguity
K_a	-	1.2	Antenna Doppler Oversample Factor to Prevent Ambiguity
ρ_r	m	0.1016	Slant-range Resolution (4 in.)
ρ_a	m	0.1016	Cross-range Resolution (4 in.)
λ_c	m	0.018	Center Wavelength
ψ_B	°	30	Nominal Broadside Grazing Angle
θ_s	°	90	Nominal Squint Angle at Aperture Center
θ_{s_range}	°	(45:135)	Possible Squint Angle Range at Aperture Center
H	m	1524	Above Ground Level Platform Altitude (5 kft)
L_a	m	0.1524	Physical Antenna Length (6 in.)
W_a	m	0.1524	Physical Antenna Width (6 in.)
τ_{antpt}	s	0.15	Time to Point Antenna to MCP
v_{TAS}	m/s	30.8667	Platform True Air Speed (60 knots)
w	m/s	0	Wind Speed
θ_w	°	0	Wind Direction Relative to Path
x_{gps}	m	10	Patch Overlap Allowance for GPS error
τ_{turn}	s	240	Maneuver Time for Platform to Turn (4 minutes)
$\tau_{mission}$	s	14400	Mission Duration (4 hours)
$Y_{\min\_seg}$	m	450	Minimum Area Coverage Segment Width
$X_{\max\_seg}$	m	15000	Maximum Area Coverage Segment Length (15 km)
$Flag_{hop}$	-	1	Allows Hopping Maneuvers if Equal to 1

DISTRIBUTION

Electronic copies delivered to:

1	MS0509	K. D. Meeks	5300
1	MS0519	D. L. Bickel	5344
1	MS0519	A. M. Raynal	5344
1	MS0519	J. A. Ruffner	5349
1	MS0519	A. W. Doerry	5349
1	MS0532	J. J. Hudgens	5340
1	MS0532	B. L. Burns	5340
1	MS0532	W. H. Hensley	5344
1	MS0533	S. Gardner	5342
1	MS0533	J. D. Bradley	5342
1	MS0533	D. G. Thompson	5342
1	MS0899	Technical Library	9536

"That which causes us trials shall yield us triumph: and that which make our hearts ache shall fill us with gladness. The only true happiness is to learn to advance, and to improve: which could not happen unless we had commenced with error, ignorance, and imperfection. We must pass through the darkness, to reach the light."

- *Albert Pike*

Sandia National Laboratories